Semi-distributed lumped model of a karst system under active management

Bernard Ladouche, Jean-Christophe Maréchal, Nathalie Dörfliger

▶ **To cite this version:**

Bernard Ladouche, Jean-Christophe Maréchal, Nathalie Dörfliger. Semi-distributed lumped model of a karst system under active management. Journal of Hydrology, 2014, 509, pp.215-230. 10.1016/j.jhydrol.2013.11.017 . hal-00905925

HAL Id: hal-00905925

https://brgm.hal.science/hal-00905925

Submitted on 18 Nov 2013

HAL is a multi-disciplinary open access archive for the deposit and dissemination of scientific research documents, whether they are published or not. The documents may come from teaching and research institutions in France or abroad, or from public or private research centers.

L'archive ouverte pluridisciplinaire **HAL**, est destinée au dépôt et à la diffusion de documents scientifiques de niveau recherche, publiés ou non, émanant des établissements d'enseignement et de recherche français ou étrangers, des laboratoires publics ou privés.

Semi-distributed lumped model of a karst system under active management

Bernard LADOUCHE[1*], Jean-Christophe MARECHAL[1] and Nathalie DORFLIGER[2]

1. BRGM, Water Environment & Ecotechnologies Division, 1039 rue de Pinville, F-34000, France Montpellier, France. http://www.brgm.fr; b.ladouche@brgm.fr; jc.marechal@brgm.fr
2. BRGM, Water Environment & Ecotechnologies Division, 3 avenue Claude Guillemin, BP 36009 F-45060 Orléans cedex 2, France. n.dorfliger@brgm.fr

*corresponding author: Tel.: 334 67 15 76 80; Fax: 334 67 15 79 75

Abstract

In this paper inverse modeling is used to characterize the regime of a karst aquifer subjected to extensive pumping in a conduit located upstream of its main outlet. The systemic approach uses a transfer model that is based on computing the convolution integral of up to several signals, e.g., efficient rainfall, pumping, to simulate flow rates and groundwater levels in both the karst conduit and the carbonate matrix at the aquifer outlet and in several parts of the catchment area. The model is a semi-distributed lumped model which simulates the hydrological response of a heterogeneous karst aquifer made up of different hydrologic compartments, and is applied to the Lez karst system, France. Groundwater is abstracted near the system's major outlet at a higher rate than the low-water spring discharge, thereby mobilizing stored groundwater during low-water periods ('active management').

The model's results are very satisfactory, especially for the karst system outlet, where the water levels are particularly well reproduced. The model can also simulate the natural, i.e., non-pumping,

state of the karst system and thereby estimate the impact of active management on the water resource.

Highlights

Characterization of karst functioning using a lumped semi-distributed approach

Interpretation of a very long times series of groundwater levels in a karst system

New insights on the mobilization of stored reserves by pumping within a karst system

Keywords

Impulse response

Groundwater flow modeling

Groundwater level fluctuations

Pumping

Introduction

Numerical models for karst aquifers usually fall within two main categories (Goldscheider and Drew 2007): lumped-parameter or reservoir models (Dreiss 1983; Pinault et al., 2001a, b, 2004) and distributed physical models (Birk et al., 2003; Liedl et al., 2003). Owing to the high degree of heterogeneity of karst aquifers, distributed models (Birk et al., 2000; Teutsch and Sauter, 1998) can be relatively difficult to implement and calibrate because of difficulties in obtaining the necessary input data. These difficulties have limited the use of such models in karst hydrogeology. Dual-porosity models with implementation of discrete pipe networks within a limestone matrix (Cornaton

and Perrochet, 2002) represent a promising approach for testing hypotheses on the conceptual representation of water interactions between the matrix and pipe networks. However, because the available data on karst conduit geometry are generally very limited, this modeling approach is difficult to implement. The lumped-parameter model is simpler and considers the karst as a whole; it uses the relationship between rainfall and discharge (bivariate analysis) to characterize the karst flow regime, and can potentially be used for a karst hydrosystem in which these data are available (Denic-Jukic and Jukic 2003; Dorfliger et al., 2009; Padilla and Pulido-Bosch 2008; Jukic and Denic-Jukic 2009; Martínez-Santos and Andreu 2010, Moussu et al., 2011, Long and Mahler, 2013). However, some karst aquifers are characterized by geographical or hydrogeological subsystems that can be considered as homogeneous units at the scale of interest which potentially are hydraulically connected to each other at the scale of the karst catchment area. In such cases, a lumped parameter model applied to the overall catchment cannot take this hydrodynamic heterogeneity into account. One option, if the necessary data are available, is to consider a lumped parameter modeling approach for each subsystem and then to aggregate the results in order to represent the overall flow regime of the karst aquifer at its outlet. This is an intermediate approach between the lumped parameter model and the distributed physical model, and here is termed a semi-distributed lumped parameter model.

Karst aquifers can form major groundwater reservoirs (Bakalowicz 2005) and are locally pumped to meet growing drinking-water requirements due, in particular, to population growth. ‘Active management’ through pumping from the main karst conduit in the vicinity of its outlet enables optimal exploitation of a karst groundwater by avoiding the negative effects of large low-water discharge variations at the springs. Active management can thus be defined as pumping at a flow rate greater than the spring’s low-water discharge rate so as to mobilize the aquifer’s stored reserves (Avias 1995). These reserves are then replenished during the following rainy season, resulting in less intense floods at the start of the season (Fleury et al. 2008). In such cases the karst system is

67 characterized by two distinct types of flow regime: (i) a high-water flow regime when the natural
68 outlet discharge is greater than the pumping rate and the system functions naturally; and (ii) a low-
69 water flow regime when the natural outlet discharge is lower than the pumping rate, and the
70 pumped flow rate is the sum of the natural outlet discharge plus the mobilized karst storage flow
71 desaturating the conduits and the matrix (Maréchal et al., 2008). Generally, when a karst system has
72 been exploited over a long period, no observations of the system's natural flow regime are available
73 and it is therefore difficult to reconstruct the system's 'natural' rainfall–discharge relationship: this is
74 a similar to attempting to determine hydrological processes in ungauged basins (Sivapalan 2003).

75 The Lez spring karst system, in southern France, has been an ideal site since the 1970s for studying
76 and modeling a flow regime. Most of the numerical models developed for studying the aquifer's
77 hydrodynamics with a view to groundwater exploitation are based on the laws for draining several
78 reservoirs (Guilbot 1975; Thiery et al., 1983, Fleury et al., 2008). These models are thus unable to
79 describe the functioning of the various hydrogeological units of the hydrosystem, and especially that
80 of the western compartment of the Matelles Fault (Massili 2011; Massili et al, 2011). The main aim of
81 our work here was to develop a lumped parameter modeling approach suitable for (i) a karst system
82 whose overall flow regime results from the juxtaposition of identified subsystems, and (ii) a system
83 that was under 'active management' for a long period of time and for which the natural flow regime,
84 in particular at the outlet, is unknown. The final objective of this work was to develop a modeling
85 approach that is able to predict the water levels and spring discharge so that the impact of global
86 change scenarios on the Lez karst system could be assessed.

87 Study area

88 The Lez karst system forms part of the North Montpellieran Garrigue hydrogeological unit delimited
89 by the Hérault river (to the west) and the Vidourle river (to the north and east, Figure 1). The Lez
90 karst aquifer, between 650 and 800 m thick, lies within the Upper Jurassic layers on both sides of the

Matelles-Corconne Fault (here termed the 'Matelles Fault'). The aquifer is unconfined in the western compartment of this fault and locally confined in the eastern compartment (Figure 2a). The base and top of the Lez karst aquifer in the eastern compartment are respectively Callovian–Oxfordian marls (Middle Jurassic) and a thick succession of Lower Valanginian (Lower Cretaceous) marls and marly limestone; the aquifer itself straddles in the Upper Jurassic and the Berriasian (Lower Cretaceous). The karstification of the main conduit below its top wall in the eastern compartment was confirmed as -10 m (a.s.l.) by diving, and down to -48 m (a.s.l.) by drilling (Figure 3). The geometry of the conduit is known only between the spring and a few boreholes located 400 meters away: this lack of knowledge at the watershed scale prohibits the application of any distributed modeling approach. A southward structuring of the aquifer, with the development of karstification at depth and an underground drainage in the direction of the Mediterranean, is probable and almost certainly related to the Messinian salinity crisis (Clauzon et al., 2005; Avias 1992). However, the compressive tectonics of the Eocene Pyrenean–Provençal phase, in addition to filling the paleo-outlet with impermeable Miocene and Pliocene sediments from the Messinian canyons, gave this large karst aquifer a 'confined karst' character with the presence of upstream overflow springs, such as the Lez spring and the intermittent Lirou spring.

The Lez spring with its overflow at 65 m (a.s.l.) is the main outlet from the karst system. The area of the hydrogeological catchment is estimated to be 380 km², based on the geology, identification of the impervious structural limits, dye tracings, and groundwater level dynamics in the network of observation boreholes during the drawdown in the spring's conduit (Thiery et al., 1983, Figure 1). Several recharge zones can be identified within this basin according to the nature of the exposed geological formation: (i) the Jurassic limestone outcrop (between 80 and 100 km^2) is the main area of recharge from effective rainfall (Figure 1); (ii) the Cretaceous marly-limestone formations (120 km²), which are much less permeable than the Jurassic, provide leakage to the underlying Jurassic and contain identified loss zones with direct recharge to the underlying Jurassic aquifer from surface

streams (swallow holes) and in particular along tectonic faults; (iii) the Tertiary formations (160 km²), which are generally impervious and which contribute insignificantly to the karst aquifer recharge.

The Lez spring has been supplying the city of Montpellier since 1854. Prior to 1968, the resource was exploited through spring overflow collection, which ranged between 25 and 600 l/s (Paloc 1979). From 1968 to 1982, abstraction was carried out by pumping in the panhole at a rate of some 800 l/s. This period was the prelude to 'active management' of the Lez karst system, with pumping rates in the summer periods being greater than the natural discharge without any pumping. By the end of the 1970s increased demand for drinking-water supply had motivated the managers to extract the resource at a rate higher than 800 l/s. For this reason, in 1982 deep wells were drilled into the main karst conduit upstream of the spring in order to obtain a maximum yield of 2000 l/s (Avias 1995). The current pumped rates at the low-water stage (between 1200 and 1700 l/s) are greater than those pumped at high water (900 l/s). The maximum pumping rate is now fixed at 1700 l/s so that the minimum water level (Figure 4) is no lower than 35 m.a.s.l., i.e., 30 m below the elevation of the spring's outlet. A reserve flow of 160 l/s returns to the Lez River downstream of the spring when the spring is not overflowing.

The karst system's natural discharge (Qn) is unknown, because the Lez spring has been tapped since 1854 (Paloc 1979). However, the pumping rate (Qp) has been measured since 1974 and the spring's residual overflow discharges (Qr) were reliably measured between 1987 and 2007. The natural high-water flows over this period can be estimated by the equation Qn = Qr+Qp (Figure 3a) —the natural discharges (Qn) estimated from these measurements are shown in Figure 5a.

At low-water stage (Figure 3b), the pumping rate (Qp) is between 1200 and 1700 l/s, which is higher than the natural discharge (Qn) would have been in the absence of pumping. The pumping caused the spring to dry up (Qr = 0). Accordingly, the pumped discharge (Qp) during the low-water period is interpreted as the sum of the flow that would have occurred naturally in the absence of pumping

(Qn) and the storage flow (Qs) mobilized by the pumping: Qp = Qn+Qs. The yield obtained from the karst storage (Qs) is interpreted as coming from depletion of the karst conduits and mobilization of matrix water from the carbonates in which the karst drainage network has been developed (Maréchal et al, 2008). Pumping thus mobilizes the karst system's water reserves that are barely or not at all accessible under the karst's natural flow regime. This is reflected in a lowering of the piezometric head (H4) in the karst conduit (35 m < h4 < 65 m a.s.l.; Figure 3b).

The Suquet borehole (Figure 2a) intersects the karst conduit connected to the Lirou spring, which is the main outlet from the Western compartment of the Lez karst system (Paloc 1987): it thus enables a description of the overall hydrodynamics of this part of the system. During high-water periods (H2 > 65 m.a.s.l.) the groundwater-level response to effective rainfall recharge is very similar to that recorded at the Claret observation borehole. This is located in a conduit in the immediate vicinity of the Matelles Fault (Fig. 1), which is one of the main drainage axes of the karst system (Lacas 1976; Drogue and Grillot 1976; Bérard 1983; Karam 1989). During low-water periods (h2 < 65 m.a.s.l.), groundwater-level monitoring reveals the existence of a 'groundwater disconnection' between the two aquifer compartments located on either side of the Matelles Fault (Figure 4). The groundwater level in the western compartment (Suquet borehole) is no longer influenced by drawdowns caused by pumping when the groundwater head of the karst conduit at Claret is 53.5 m.a.s.l. or 52 m.a.s.l. at the Lez observation borehole (Figure 4). The measured groundwater levels at the Suquet observation borehole can be explained if one considers that a 'cascade'-type disconnection exists in the conduit. This does not preclude a water flow from the western compartment continuing to supply the Jurassic located below the Cretaceous cover in the eastern compartment, but the two hydraulic heads measured on either side of the Matelles Fault are independent. The Suquet observation borehole is representative of the karst system draining the western compartment of the Matelles Fault.

The groundwater level H3 measured in the Laudou observation borehole (Figure 1) also appears to be influenced by the pumping (Conroux 2007); but indicates a different hydrodynamic response from

the conduit (Lez, Claret, Figure 4), which exhibits a much more inertial groundwater behavior (Conroux, 2007), one that we assume is representative of the matrix storage beneath the Cretaceous cover to the east of the Matelles Fault (Figure 2a).

Semi-distributed lumped model

The semi-distributed lumped modeling approach developed for the present study is based on the state of knowledge concerning the Lez karst system. The architecture of the hydrological model is shown in Figure 2b. Four sub-models (or modules) was used to reproduce the hydrodynamic flow regime of a complex karst aquifer, composed of two compartments (the western and eastern parts of the Matelles fault), and subjected to an 'active management' through pumping at the Lez spring (Figure 2a). The first three modules simulate (i) the natural discharge of the Lez spring (Qn), and the water levels in (ii) the karst conduit of the western compartment at the Suquet observation borehole (ΔH2) and (iii) the matrix of the eastern compartment at the Laudou observation borehole (ΔH3). The fourth module calculates the groundwater level of the main karst conduit at the Lez spring (ΔH4) from the contributions (outputs) of the three intermediate transfer modules.

The hydrogeologic modeling was performed using transfer methods implemented with TEMPO software (Pinault, 2001). The calculation of the impulse responses of the transfer modules is achieved by inverse modeling with stress positivity. The term inverse modeling is here restricted to the parameter identification of convolution kernels used to simulate the output from the input. Computation of the impulse response uses regularization methods inspired by Tikonov and Arsenime (1976), Tikonov and Goncharsky (1987), and Dietrich and Chapman (1993), as described by Pinault et al. (2001a). The calculation of impulse responses under stress allows to satisfying the principle of conservation of the water mass. The impulse responses can be parametric or non-parametric. In the case of a non-parametric impulse response, the system is termed ill-posed from a numerical point of view because it has an infinite number of solutions. As mentioned by Doherty and Skahill (2006), the so-called "Tikhov regularization", in which the parameter estimation process is formulated as a

constrained minimization problem, enables an efficient and stable solution to the inverse problem to be obtained. The mathematical and numerical bases used in Tempo software for the calculation of impulse responses are presented in Pinault et al. (2001a). The search for a solution by the regularization technique seeks to reduce the number of degrees of freedom of the optimization problem by minimizing the norm of the transport equation (i.e eq. 7, eq. 9, eq. 11 and eq. 13 in this study). Among all possible solutions, the calculation of minimizing the norm of the solution aims to select the one with the smallest norm in order to smooth the non-parametric impulse response. As indicated by Pinault et al. (2001a), the regularization parameter (w) is optimized by using the method of the curve L. This technique takes its name from the shape of the curve obtained when the x-axis represents the norm of the solution and the y-axis the difference between the model and the observations. The regularization parameter (w) is selected as close as possible to the angular points of the curve L. This choice is a compromise between (1) choosing a very smooth solution which produces a poor fit, and (2) choosing a very irregular solution producing an excellent fit between the model and the observations. The regularization parameter (w) is the absolute value of the derivative of the curve L. The second parameter of the non-parametric impulse response is the maximum length over which the computation is performed.

The modeling approach using Tempo software enables a characterization of the flow regime of complex hydrosystems such as those found in karst systems (Pinault et al., 2001b, 2004; Dörfliger et al., 2009) as well as in more homogeneous porous media (Pinault et al. 2005; Pinault and Schomburgk 2006; Pinault and Allier 2007).

Effective rainfall

The modules use the same daily input data to compute the effective rainfall, with the possibility of using several rain gauges (*p* being the number of rain gauges) for the rainfall data:

$$R_{\Sigma} = \sum_{k=1,p} \delta_k R_k \qquad \delta_k \geq 0 \; k = 1, \dots, p \qquad \sum_{k=1,p} \delta_k = 1$$

The sum R_Σ of a series of rainfall data is defined so as to optimize the contribution of each rain gauge to the transfer model of the spring's discharge (Module 1). The principle, given by Pinault et al. (2005) consists of computing the weighting factors (δk) of the rain gauges so that they maximize the cross-correlation between rainfall and system output.

The amount of effective rainfall $R_{eff}(t)$ inducing a flow variation for a time t is calculated by:

$$R_{eff}(t) = R_\Sigma(t) - \Omega(t) \; if \; R_\Sigma(t) \geq \Omega(t) \; otherwise \; R_{eff}(t) = 0 \qquad \text{Eq. 1}$$

The effective rainfall (R_{eff}) is calculated by computing the threshold function Omega:

$$\Omega(t) = Gr * R_\Sigma(t) + GTa * Ta(t) + C \qquad \text{Eq. 2}$$

where * is the discrete convolution product, *t* the time, *C* a constant, and *Gr* and *GTa* the impulse responses such that *GTa* > 0 and *Gr* < 0. These two impulse responses (*Gr* and *GTa)* are represented by trapezia (Figure 5c). Details of the impulse response parameter calculation are presented in Pinault et al. (2001a).

The threshold **Ω***(t)* is used to express the deficit of the effective reserve in the ground. Rain decreases the **Ω***(t)* threshold, following the reservoir's recharge, while air temperature (*Ta*) increases it. The convolution of rain with the negative part of the impulse response (Figure 5c) gives the contribution of rain threshold Ω(t). The threshold **Ω***(t)* (Eq. 2) can be computed using the air temperature (Ta) because the input and output variables are reduced (divided by their mean). Consequently, only the variations are involved and it is these that determine the model's accuracy (Pinault 2001). The air-temperature records used in the calculation (Eq. 2) are from the St-Martin de Londres meteorological gauging station (Figure 1).

The effective rainfall $R_{eff}(t)$ is divided into two components: $R_{eff}(t) = R_s(t) + R_f(t)$, where $R_s(t)$ and $R_f(t)$ are the components of effective rainfall that respectively induce the slow and fast responses of the

system. The fast component is assumed to be representative of the fast infiltration which occurs only after high-rainfall events. The component $R_f(t)$ is expressed according to $R_{eff}(t)$ by the Alpha function [$\alpha(t)$]:

$$R_f(t) = \alpha(t) \times R_{eff}(t) \quad \text{Eq. 3}$$

where $\alpha(t)$ is the proportion of effective recharge (its values lie between 0 and 1). The Alpha function enables consideration of the non-linear switching behavior of karst systems such as 'Flush flow' which depends on the effective rainfall over the preceding days. The Alpha function is related to the effective recharge by the convolution product:

$$\alpha(t) = \Gamma_{\alpha,\mathrm{Re}\,ff} * R_{eff}(t) \quad \text{Eq. 4}$$

where * is the discrete convolution product, *t* the time, and $\Gamma_{\alpha,\mathrm{Re}\,ff}$ the impulse response of $\alpha(t)$ to effective rainfall $R_{eff}(t)$. The impulse responses are represented by trapezia (Figure 5d).

Module 1: Transfer model for the rainfall –Lez spring natural discharge relationship

The first module (Figure 2b) computes the natural discharge of the Lez spring (Qn) which would flow naturally in the absence of pumping and the mobilized storage flow (Qs). Inverse modeling of the natural flow consists of calculating both the slow (τs) and fast (τf) impulse responses associated with the different types of flow that occur within the karst system. The fast transfer (τf) may be associated with 'flush flow'. This can occur when hydraulic continuity is established between the unsaturated and saturated zones of the karst through a temporary connection between groundwater in the epikarst and the saturated zone, via fractures and/or subvertical conduits (Pinault et al., 2001b). 'Flush flow' has been demonstrated in the Fontanilles and Cent-Fonts karst systems to the north of Montpellier (Aquilina et al., 2005, 2006) during periods of major recharge. The impulse response of the fast flow (τf) can also describe the contribution of losses from temporary streams

located in the catchment area of the Lez spring. In the model, the fast transfer of the recharge (τf) is obtained by the convolution product of a Gaussian function with a decreasing exponential:

$$\begin{cases} \tau f(t_i) = A.exp\left(-\ln(2)\left(\frac{(t_i\ -T)}{D}\right)^2\right) * \exp\left(\frac{-t_i\ \ln(2)}{L}\right)\ if\ 0\ \leq t_i \leq \tau \\ \tau(t_i) = 0\ if\ t_i > \tau \end{cases} \quad \text{Eq. 5}$$

From a physical viewpoint, the model reflects the recharge of a reservoir (Gaussian function) followed by its rapid depletion represented by the decreasing exponential law. The succession of these two phenomena is described by the convolution product (*). The parameter *T* expresses the delay of the recharge process with respect to the rainfall, while the parameter *D* reflects the duration of the event. *A* is the normalization constant.

The slow transfer (τs) brings into play the various infiltration and depletion processes inducing a more-or-less significant delay between the rainfall and the observed discharge. The depletion of the saturated zone is also described by this slow transfer. In the approach we adopted, the slow transfer of the recharge (τs) is described by a parametric model (Denic-Jukic and Juckic 2003) that convolves an analytical function consisting of two reservoirs in parallel, and the depletion of the saturated zone is described by a decreasing exponential function. The choice of this type of parametric model can be justified by the existence of the two karst compartments located on either side of the Matelles Fault. The expression for the two unequal parallel linear reservoirs with recession coefficients *k*1 and *k*2 is:

$$\tau s = \frac{\theta}{k1} e^{-t/k1} + \frac{1-\theta}{k2} e^{-t/k2} \quad \text{Eq. 6}$$

where the parameter θ represents the flow ratio between the two reservoirs. The impulse response is presented on Figure 5e.

The discharge *Qn(t)* is computed by the following equation (Eq. 7):

$$Qn(t) = A\ (\tau f * Rf + \tau s * Rs) \quad \text{Eq. 7}$$

Where * represents the discrete convolution product, *t* the time, *Qn(t)* the flow of the hydrosystem, *A* the recharge area of the catchment basin (where recharge occurs), τf and τs the normalized impulse responses (the area being the unity), and *Rf* and *Rs* the components of the effective rainfall (*Reff* = *Rf* + *Rs*) inducing the fast and slow transfers respectively. The inverse modeling process calculates the normalized impulse responses τs and τf, the effective rainfall [$R_{eff}(t)$], and the part of effective rainfall [$\alpha(t)$] that is involved in quick flow.

The karst storage flow (*Qs*) mobilized by the pumping is then calculated as follows:

$$\begin{array}{l} if\ Qp \geq Qn\ then\ Qs = Qp - Qn\ \ and\ Qr = 0 \\ if\ Qp < Qn\ then\ Qs = 0\ \ and\ Qr = Qn - Qp \end{array} \qquad \text{Eq. 8}$$

where *Qs* represents the karst storage flow, *Qp* the pumping rate, and *Qn* the natural flow in the absence of pumping. The karst storage flow (*Qs*) is negative (by convention) and is assumed to be zero when there is overflow at the outlet (high water). The karst storage volume *Vs* calculated from *Qs* is different from the dynamic volume *Vd* which would have flowed in the absence of pumping, the latter generally being assessed from the analysis of recession curves (Mangin 1975).

Module 2: Transfer model for the rainfall – Lirou spring discharge relationship (Western compartment)

The second or Suquet module (Figure 2b) simulates the hydraulic head of the conduit (ΔH_2) in the Jurassic compartment west of the Matelles Fault (Suquet borehole; Figure 1 and Figure 2a) near the Lirou overflow spring. The relationship between the recharge (input) and the piezometry (output) is based on computing a non-parametric impulse response

$$H2(t) = \frac{1}{\eta 2}\, \Gamma_2 * R_{eff} + \varepsilon \qquad \text{Eq. 9}$$

where Γ_2 is the normalized impulse response (area equal to 1) of the effective rainfall recharge and $\eta 2 = Ws \times Max\ (\tau_2)$, a constant linked to the porosity (*Ws*) through determination of the base

piezometric level H_0 (Pinault 2001) and the maximum value of the normalized impulse response (τ_2); ε represents the erratic contribution that is not described and explained by the model. The computation of the impulse responses is performed under positivity constraint and while satisfying the principle of conservation of the mass of water, the groundwater level being expressed relative to a reference level H0. This reference level is the groundwater level in the absence of external solicitation (effective recharge, pumping). The inverse modeling is set up to calculate the normalized impulse response [Γ_2] (Figure 6c), the threshold **Ω***(t)* (Figure 6b), and the effective rainfall. Parameters are obtained through inversion by minimizing the quadratic form:

$$\sum_{i=1}^{N} \left(H2_{obs}(t_i) - H2_{mod}(t_i)\right)^2 \qquad \text{Eq. 10}$$

The slow component can reproduce the hydrological response of the western compartment (Figure 6c). The fast component is not necessary for this module.

Module 3: Transfer model for the matrix storage (Eastern compartment)

The third or Laudou module is used to characterize the functioning of the Jurassic karst beneath the Cretaceous cover (Figure **2**b) in the eastern compartment of the Matelles Fault. This transfer model takes into account the recharge by effective rainfall as well as the effect of the karst storage flow (Qs) mobilized by pumping.

The piezometric evolution is described by the following convolution equation:

$$H3(t) = \frac{1}{\eta 3}.\Gamma_3 * R_{eff} + \lambda_{3s}.\Gamma_{3s} * Q_S + \varepsilon \qquad \text{Eq. 11}$$

where Γ_3 and Γ_{3s} are the normalized non-parametric impulse responses (areas equal to 1), Γ_3 is the normalized impulse response of the recharge from effective rainfall, and Γ_{3s} is the normalized impulse response of the mobilized karst storage flow; ε represents the erratic contribution that is not described and explained by the model. The parameters $\frac{1}{\eta 3}$ and λ_{3s} are positive coefficients for expressing the conservation of the water mass:

$$\frac{1}{\eta 3}.\frac{\overline{R_{eff}}}{\overline{\Delta H3}} + \lambda_{3s}.\frac{\overline{Q_S}}{\overline{\Delta H3}} = 1 \qquad \text{Eq. 12}$$

The term $\frac{1}{\eta 3}.\overline{R_{eff}}$ is used to describe the relative contribution of the recharge and $\lambda_{3s}.\overline{Q_S}$ describes the relative decrease in piezometry resulting from the karst storage flow (Q_S) mobilized by pumping in the conduit of the Lez spring.

The inverse model of fissured matrix storage in the Jurassic karst beneath the Cretaceous cover is represented in Figure 7. The inverse modeling calculates the threshold **Ω***(t)* (Figure 7b) and the effective rainfall, the normalized impulse response of the recharge (Γ_3), and the normalized impulse response of the karst storage flow mobilized by pumping (Γ_{3s}). The impulse responses of the two contributions $\Gamma_3 \text{and } \Gamma_{3s}$ are shown in **Figure 7**b. The computation of the impulse responses is performed under positivity constraint, the groundwater level being expressed relative to a reference level H0. The fast component is not necessary for this module.

Module 4: Transfer model for the main conduit to the Lez springhead

Module 4 (Figure **2**b) enables a simulation of the water level of the Lez karst conduit in the immediate vicinity of the spring (borehole located 400 m upstream of the Lez spring) and thus to characterize the global hydrodynamics of the system at the outlet. Module 4 is a system convolved in sequence since the outputs of Modules 2 and 3 [H2(t) and H3 (t)] are the inputs to the convolution kernel of the simulation model for the water level [H4 (t)].

The piezometry is calculated by the following convolution equation:

$$H4(t) = \lambda_a.\Gamma_a * R_{eff} + \lambda_b.\Gamma_b * Q_S + \lambda_c.\Gamma_c * H_2 + \lambda_d.\Gamma_d * H_3 + \varepsilon \qquad \text{Eq. 13}$$

where $\Gamma_a,\ \Gamma_b,\ \Gamma_c \text{ and } \Gamma_d$ are the normalized non-parametric impulse responses (areas equal to 1); Γ_a is the normalized impulse response of the effective rainfall recharge; Γ_b is the normalized impulse response of the mobilized karst storage flow (Q_S); Γ_c is the normalized response of the supply

component from the Jurassic aquifer lying to the west of the Matelles Fault (computed by the Suquet module); Γ_d is the normalized response of the supply component from the matrix (computed by the Laudou module); and ε represents the erratic contribution that is not described or explained by the model.

λ_a, λ_b, λ_c and λ_d are positive coefficients for expressing the conservation of the water mass:

$$\lambda_a.\frac{\overline{R_{eff}}}{\overline{\Delta H4}} + \lambda_b.\frac{\overline{Q_S}}{\overline{\Delta H4}} + \lambda_c.\frac{\overline{\Delta H_2}}{\overline{\Delta H4}} + \lambda_d.\frac{\overline{\Delta H_3}}{\overline{\Delta H4}} = 1 \qquad \text{Eq. 14}$$

The term $\lambda_b.\overline{Q_S}$ allows us to describe the relative decrease caused by the mobilized karst storage flow (Q_S). The term $\lambda_c.\overline{\Delta H_2}$ describes the relative contribution of the Jurassic aquifer on the west of the Matelles Fault. The term $\lambda_d.\overline{\Delta H_3}$ allows us to describe the relative contribution from the matrix reservoir. In this model, the term $\lambda_a.\overline{R_{eff}}$ does not allow a description of the contribution from the effective rainfall; we fixed this parameter at 1% because we consider that most of the effective rainfall recharge information is already contained in the model's other components (ΔH_2 and ΔH_3). This component enables one to describe the recharge phenomena associated with the fast flow that occurs during significant flooding (Q>3000 l/s). We assume that the component described refers to direct infiltration from losses associated with the temporary streams that form during floods.

Results

Rainfall data from three weather stations were used (Fig. 1): Saint-Martin de Londres (R1), Montpellier-Fréjorgues (R2), and Valflaunes (R3). The aim of the computation was to maximize the cross-correlation between R_Σ and the overflow discharge (Qr) at the Lez spring measured between 1987 and 2007. The linear combination obtained for R_Σ is:

$$R_\Sigma = 0.34*R1 + 0.53*R2 + 0.13*R3 \qquad \text{Eq. 14}$$

The calibration of Module 1 was based on the natural high-water discharges (Qn = Qr+Qp for the period 1998-2006; Figure 5a); the natural low-water discharges are not known. The parameters of the transfer function (Eq. 6) shown on Figure 5e are: $k1$ = 7.4 days, $k2$ = 59 days, $\theta = 0.29$. The length of the impulse response is 324 days. The mean transit time (Tm) associated with the normalized impulse response is the mean value of the lag (Pinault et al, 2005). The average transit time (Tm) is 42 days. The first transfer model assumes that the regulation time (system memory) of the slow component of the karst system is less than a year (324 days; Figure 5e). This assumption is not restrictive because the karst system's spring begins to flow again with the first autumnal rains, and the low-water periods (recession) do not exceed a year. The model was validated with the natural high-water discharges for the 1987–1997 period (Figure 5b); it satisfactorily reproduces the high-water periods, and the Nash criterion of 0.67 (Nash and Stutcliff, 1970) is considered satisfactory, having been calculated on the high-water cycles for the 1987–2007 period. The area of the karst catchment basin providing recharge is estimated at 116 km^2. The fast component (Qf) of the recharge flows only during significant floods (Qn > 3000 l/s) and contributes up to a maximum 7% of the flood discharge.

For Module 2, the reference level is that measured at low water when the head becomes constant (H_0= 60 m.a.s.l.) following groundwater-level disconnection from the Jurassic compartment lying east of the Matelles Fault. The groundwater level is described only by the slow component of the recharge, the fast component being unnecessary for the simulation. The impulse response for the slow component is shown in Figure **6**c. The average transit time (Tm) of the normalized impulse response (τ_2) is 42 days. The regularization parameter (w) is 0.1. The length of the impulse response is 96 days. Module 2 enables a satisfactory reproduction of the daily changes of the groundwater level measured at the Suquet observation borehole (high Nash criterion = 0.88). The model was validated with the water levels measured for the 2011–2012 period (Figure 6c): it satisfactorily reproduces the high-water and low-water periods, and the Nash criterion of 0.82 is considered

satisfactory. The model nevertheless tends to overestimate the groundwater level after the first floods of the new hydrological cycle (autumn). The effective porosity ($\eta 2$) is estimated at 0.37%, which is a general value for the aquifer compartment drained by the Lirou overflow spring; the Suquet observation borehole taps the same drainage system just upstream of the intermittent spring. This second transfer model was used to simulate the groundwater level of the western compartment (1974–2010; Figure 9e) and the output of this module 2 modeling is one of the inputs to the fourth module of the Lez transfer model.

In Module 3, computing the effective porosity ($ws = \eta 3/Max[\Gamma]$) requires a knowledge of the base level (H_0) corresponding to the piezometric level reached by the system in the absence of recharge and pumping (Pinault 2001, Pinault et al., 2005). Because in the present case the base level (H_0) cannot be deduced from the observed piezometric record, owing to the influence of pumping, it was characterized using the model using trial and error to obtain a maximum Nash criterion. The base level obtained is H_0= 80 m.a.s.l., which is an intermediate value in the observed variation range (61–115 m.a.s.l.). The effective porosity ($\eta 3$) is estimated at 0.91%. The average transit times (Tm) of the normalized impulse responses of the two contributions ($\Gamma_3 \text{and } \Gamma_{3s}$) are 47 days and 9 days respectively (Figure 7b). The regularization parameter (w) is 0.1. The length of the impulse response is 160 days. For offsets longer than 50 days, the non-parametric impulse response of effective rainfall shows oscillations which correspond to noise without physical meaning. Nevertheless, the length of the impulse response is significant because the tests conducted with a shorter length for the impulse response do not allow the modeling of the inertial response of the aquifer to effective rainfall. This third transfer model provides a satisfactory simulation of the daily evolution of the measured piezometry for the calibration period (Nash criterion = 0.82, Figure 7a). The model was validated with the water levels measured for the 2008–2011 period (Figure 5d); it satisfactorily reproduces the high-water periods, and the Nash criterion of 0.69 is considered acceptable. The average recharge contribution is estimated at about 71.5%, with the mobilized karst storage flow (Qs) explaining on

419 average 28.5% of the measured piezometric variations. When the water level drops below the
420 reference level (H_0 = 80 m), the piezometric variation appears to be controlled mainly by the
421 mobilized storage flow (Qs) component, which can thus cause drawdown in the piezometer of nearly
422 13 m. This third model was used to estimate the groundwater level within the karst for the period
423 before 2003 and for that after 2005. The record produced by this modeling forms one of the inputs
424 to the fourth module of the Lez transfer model (1974–2008; Figure 9e).

425 The impulse responses (Γ_a, Γ_b, Γ_c and Γ_d) of Module 4 were computed for the shortest possible lags
426 (4 days, Figure 8c) to make the model stable, since the H2(t) and H3(t) variables are strongly
427 correlated (Figure 10). The average transit times (Tm) of the normalized impulse responses of the
428 two contributions Γ_a and Γ_b are 2.5 days and 2 days respectively, but are less than 1 day (0.9 day) for
429 contributions $\Gamma_c$and Γ_d. The regularization parameter (w) is 0.1 and the length of the impulse
430 response is 4 days. The reference level H_0, estimated by trial and error so that the model would be as
431 close as possible to the observed groundwater level, is H_0= 59.9 m.a.s.l. Note that this reference level
432 is similar to that obtained by the Suquet method (H_0=60 m) which reflects the moment when the
433 karst west of the Matelles Fault is piezometrically disconnected from the rest of the aquifer located
434 beneath the Cretaceous cover.

435 The model gives a very satisfactory reproduction of the daily changes of the measured groundwater
436 level (calibration period from 29/04/2002 to 25/02/2004) with a Nash criterion of 0.97 (Figure **8**a)
437 and a very low standard deviation (0.02). The model has been used to simulate the groundwater
438 level of the karst conduit for the periods before 2002 and after 2004 (Figure 9e). The model was
439 validated with the water levels measured before 2002 (1974–2002 period) and after 2004 (2004-
440 2011 period) (Figure 5a). This transfer model gives a satisfactory simulation of the daily changes of
441 the water level measured in the conduit (Nash criterion = 0.68). The periods of aquifer drawdown
442 corresponding to the spring drying up are well reproduced. The simulated flood water levels are in
443 some cases greater than the measured levels.

Most of the groundwater level variation (44%, Figure **9**b) relative to the reference level (H_0=59.9 m.a.s.l.) appears to be explained by the impulse response of the mobilized karst storage flow (Qs). The average contribution of the matrix reservoir to the groundwater-level variation in the karst conduit is around 36%. The remaining part (20%) comes from the contribution of the karst lying west of the Matelles Fault. When the groundwater level in the conduit falls below 59.9 m.a.s.l. (reference level), the groundwater level variations appear to be mainly controlled by the mobilized karst storage flow (Qs), whose average contribution becomes greater than 90%.

Discussion

Sensitivity

The time-invariant impulse response (IR) used to describe the dynamic response of a system to an instantaneous impulse can be objectively chosen as a mathematical function selected on physical grounds, or by the use of a non-parametric approach (Von Asmuth et al, 2002). In this study, the choice focused on the non-parametric approach because we believe that karst processes are not well explained by physical laws only. Indeed, the shape of the impulse response to an instantaneous impulse of recharge is the result of diffuse, fracture, and conduit flows with the potential existence of turbulent flows, themselves conditioned by vertical and horizontal heterogeneities. In order to assess the model's sensitivity to the choice of the non-parametric impulse response, rather than a parametric one, we also calibrated the transfer module of Suquet borehole with a parametric model. The convolution function used to perform the sensitivity test is a Gaussian-Exponential function (Eq. 5). Using this model, the recharge of a reservoir is described by the Gaussian function $[exp\left(-\ln(2)\left(\frac{(t_i\ -T)}{D}\right)^2\right)]$ whereas the decreasing exponential function $[\exp\left(\frac{-t_i\ \ln(2)}{L}\right)]$ allows to represent the drainage from the reservoir; the succession of these two phenomena is the convolution product of the recharge law by the discharge law. The normalized impulse response of the parametric model is reported in Figure 6c, enabling a comparison with the impulse response of

468 the non-parametric model. The non-parametric model produces a better fit than the parametric
469 model both for the calibration period (Nash= 0.88 and 0.82, respectively) and for the validation
470 period (Nash= 0.82 and 0.69, respectively, Figures 6b and 6d). The main difference concerns the peak
471 response to the effective recharge, which occurs after a delay of two days. The response of the
472 parametric model is smoothed compared to that determined by the non-parametric approach; the
473 small oscillations present on the latter for offsets longer than 16 days correspond to low-level noise
474 without physical meaning. This result demonstrates that karst phenomena are not always well
475 explained by physical laws, i.e., the parametric function. The recession of the normalized impulse
476 responses for the parametric and non-parametric functions (for lags >16 days) are very similar. This
477 result shows that the optimization procedure used in the Tempo software to calculate the
478 regularization parameter of the non-parametric function produces solutions that are smooth enough
479 to be comparared to that obtained by a model of exponential decay. These results have reinforced
480 our belief that the hydrogeological functioning of the Lez karst system would be better characterized
481 by the use of a non-parametric impulse response.

482 As outlined by Long and Malher (2013), the modeling performance can be verified by using the
483 length of the modeling's validation period. A lengthy validation period with a good fit allows us to
484 evaluate the model's ability to predict the evolution of the system under other constraints (for
485 example climate change and/or resource management scenarios). The modeling approach used in
486 this study provides a very satisfactory reproduction of the daily time series of the groundwater level
487 measured since 1974, with a Nash criterion of 0.68 and a low standard deviation (0.06). The time
488 series calculated by the model are considered generally satisfactory, especially during periods of
489 aquifer drawdown when the pumped discharge is greater than the natural discharge in the absence
490 of pumping. In retrospect, these results validate the approach of reconstructing the natural flows of
491 the Lez. Nevertheless, for some hydrological cycles, the model appears sensitive to summer rainfall
492 episodes, when the calculated groundwater level may appear higher than the measured values. For

493 the period prior to 1983, the model tends to overestimate the drawdowns, which indicates that the
494 natural discharges estimated by the modeling are probably underestimated. Indeed, we previously
495 showed that the groundwater-level time series in the karst conduit are controlled solely by the
496 impulse function of the mobilized storage flow (Figure 8b), as soon as the groundwater level falls
497 below the H_0 reference level of 59.9 m a.s.l. The under- and over-estimations of the simulated low-
498 water groundwater levels (H <65 m.a.s.l.) are therefore related to the mobilized storage flow, and
499 consequently to the natural flow estimated by modeling. An overestimation of the natural flows from
500 the Lez spring results in an underestimation of the mobilized storage flow. The transfer model
501 reflects this underestimation of Qs by simulating groundwater levels higher than the measured
502 values (as with 1992, for example; Figure 9e). Conversely, an underestimation of the natural flow
503 leads to a simulation of groundwater levels below the measured values (as with 2006, for example;
504 Figure 9e).

505 In order to assess the model's sensitivity to the estimated natural discharge, the Lez groundwater
506 level was simulated assuming that the spring discharge is known to within ±10%. The results of new
507 groundwater-level simulations show that the model is generally not very sensitive to the uncertainty
508 in the estimated Lez flow rates (figure not given). On the other hand, the results indicate that the
509 modeling bias, highlighted in some hydrological cycles, is caused by poor estimation of the effective
510 rainfall. The transfer model of Module 1 appears optimistic when significant rainfall events (H> 25
511 mm) occur during the summer low-water period. The simulated groundwater level during these
512 periods therefore appears overestimated because the simulated natural flows are overestimated.

513

514 **Area of pumping influence**

515 The area of the karst catchment in which recharge occurs is estimated to be 116 km², which
516 corresponds to the area of outcropping Jurassic limestone in the hydrogeological basin (100 km²), to

517 the contribution of occasional losses from temporary streams, and also to leakage from the overlying
518 Cretaceous. This area is comparable to the 120 km² determined by Thiery and Bérard (1983) and the
519 130 km² area parameterized by Fleury et al. (2008) in their reservoir model. The natural discharge of
520 the Lez spring estimated by modeling is 1870 l/s (2σ = 590 l/s, interannual average for the 1974–2010
521 period). Also for this period, the average interannual discharge of the residual overflow rate (Qr) is
522 1030 l/s, the pumping rate (Qp) is 995 l/s, and the mobilized storage flow (Qs) is 150 l/s.

523 The hydrogeological model developed in this study provides interesting information on the structure
524 and flow regime of the Lez karst system. When the spring dries up (H <65 m.a.s.l.), the time series of
525 the water level in a karst conduit is controlled by the mobilized storage flow, which is a function of
526 the pumping rate and the hydrogeological state of the karst in the absence of pumping (as described
527 by the natural flow of Lez estimated by modeling). The amount of drawdown as a function of the
528 volume pumped from the karst storage (Vs) is shown in Figure 11. It appears linearly related to the
529 volume of water pumped from the karst storage, the slope of the line being estimated at 112,800 m^3
530 per meter of drawdown. In the pumped section of the water column (between 35 and 65 m.a.s.l.).
531 The results do not reveal any change in the hydrodynamic parameters with depth. For the water
532 column below 35 m.a.s.l., a modification of the hydraulic parameters cannot be excluded. Only a
533 pumping test in this section of the water column would provide the answer. The equivalent area of
534 karst storage mobilized by pumping has been estimated from the slope (112,800 m^3/m ± 1800 m^3/m)
535 and the effective porosity (0.91%) calculated by Module 3, which characterizes the karst matrix
536 below the Cretaceous cover. Assuming an elliptical groundwater level surface within the matrix
537 tending toward the conduits, the area of pumping influence around the network of karst conduits is
538 estimated at 59 km², which is only a small fraction of the Lez spring's groundwater basin.

539 **Active management**

540 Hydrogeologically, reconstructing the Lez spring's natural flow makes it possible to characterize the
541 development of the aquifer's water resources since the onset of 'active management' based on

542 drilling (1983). Analysis of the reconstructed natural flows for the 1974–2010 period shows that the
543 volumes extracted annually are generally less than the annual recharge (Figure 11a). For the rainfall-
544 deficient years (1983, 1998, 2007), the pumped volumes are comparable to the volume of recharge
545 (Vp ~ Vs). The volumes of water pumped from the karst storage on average represent 18% (Vs/Vp
546 ratio) of the mean annual pumped volumes (32.3 million m^3; Figure 11b). The Vs/Vp ratio rises to
547 30% in the rainfall-deficient years. Figure 11b also clearly shows the moment at which the active
548 management of the Lez resource was modified (1983).

549 The annual trend of the different volumes (Vn, Vp, and Vs) and the Vs/Vp ratio are shown in Figure
550 12 (interannual average over the period 1983–2010). The volumes of water pumped from the karst
551 storage vary during the year (Figure 12b), with the Vs/Vp ratio being highest in August and
552 representing an interannual average of 55% of the pumped volume for this month. The interannual
553 average Vs/Vn ratio reaches 170% in August, indicating that the volume of water pumped from the
554 karst storage is much higher than the average volume of water that would have flowed naturally in
555 the absence of pumping (interannual average of +70%). The box plot (Figure 12d, e) illustrates the
556 range in variability of the calculated ratios for the summer months (July, August, and September). For
557 the rainfall-deficient years corresponding to the dry quinquennials (decile 0.8), the Vs/Vp and Vs/Vn
558 ratios are respectively 70% and 235% in August.

559 # Conclusion

560 The methodological approach developed in this study is based on breaking down the head variations
561 of a karst system subjected to pumping, and on modeling the outlet discharges using transfer
562 models. This approach has made it possible to model the groundwater level fluctuations in different
563 compartments of the Lez karst aquifer, the residual flows at the spring, and the pumped karst
564 storage flow. It is an overall semi-distributed approach enabling the aggregation of the hydrological
565 responses of the various compartments interacting with each other. It constitutes a modeling

alternative when (i) the complexity of the karst aquifer necessitates a more elaborate approach than a simple lumped model, and (ii) the data necessary for a distributed model are not available. It has also helped to reconstruct the natural flow of the spring in the absence of pumping. The uncertainty generated by this last aspect was the subject of a sensitivity analysis that showed the model to be relatively insensitive to the uncertainty in calculating the naturalized flow.

The models developed in this study reveal that the aquifer is not being overexploited. They will eventually allow the testing of various resource-management scenarios and assessments of the impacts on a) the time series of the karst system's total head (karst conduit and matrix), and b) the time series of residual flow. The data acquired will make it possible to evaluate the impacts of climate change and anthropogenic pressures on the short- and long-term water changes in the water resources, using wavelet analysis

Acknowledgements

This work was carried out under the Lez–GMU Project, in the framework of the BRGM's EAUR15 research program. The authors thank the Montpellier Agglomeration, the Water Agency Rhone-Méditerranée-Corse, and the Hérault General Council, as well as the BRGM, for their funding support.

The authors also wish to thank Barbara Malher and the anonymous referee for their helpful comments, which led to substantial improvements in the manuscript.

585

586 # Figure captions

587 Figure 1: Simplified map of the lithotectonic units in the study area. Jurassic limestone outcrops
588 correspond to the main recharge zones.

589 Figure 2: Interpretative geological cross section (NW – SE) of the Lez aquifer and architecture of the
590 models used to simulate (1) the natural Lez spring discharge from effective rainfall; (2) the water
591 level in the karst conduit (Suquet borehole) located close to the intermittent Lirou karst spring fed by
592 effective rainfall; (3) water level in the matrix (Laudou piezometer) fed by effective rainfall and the
593 storage flow (Qs) mobilized by pumping; and (4) water level in main conduit (Lez borehole) fed by
594 effective rainfall, Jurassic contribution from aquifer located west of the Matelles Fault (2), matrix
595 contribution (3), and contribution of the storage flow (Qs) mobilized by pumping.

596 Figure 3: Cross section of the karst network upstream of the Lez spring.

597 Figure 4: Changes in water levels in the karst conduit (Lez and Suquet boreholes, Claret piezometer)
598 and matrix (Laudou piezometer) for the period 2000–2009.

599 Figure 5: Module 1 - Inverse modelling of the natural discharge of the Lez spring on a daily time step.
600 The observed and modelled natural discharges for flood and high-water periods are plotted for both
601 the calibrated period (a) and simulated period (b). The Nash coefficient is 0.67 for the high waters of
602 the 1987–2007 period. The natural discharges for the low-water periods are calculated from the
603 impulse response of the slow component (e). The impulse responses of the infiltration threshold
604 $\Omega(t)$ to rainfall and air temperature are also plotted (c, d), as are the slow and fast normalized
605 impulse responses of the effective recharge (e, f).

606 Figure 6: Module 2 - Inverse modeling of the water level in the karst conduit located close to the
607 intermittent Lirou spring (Suquet borehole) on a daily time step. (a) Infiltration threshold used in
608 calculating the effective rainfall. (b) Comparison between the observed and modeled water levels
609 from non-parametric model. (c) Slow normalized impulse response to effective rainfall (the fast
610 impulse response not detected) for non-parametric and parametric models. (d) Water level
611 simulated for the 2000–2012 period.

612 Figure 7: Module 3 - Inverse modeling of the matrix water level (Laudou piezometer) on a daily time
613 step. (a) Comparison between the observed and modeled water levels. (b) Slow normalized impulse
614 response to effective rainfall (fast impulse response not detected) and impulse response to the
615 mobilized karst storage flow (Qs). (c) Hydrograph separation of the two water-level related
616 components (Fig. 2) – piezometric variations are expressed relative to the reference level (H_0 = 80
617 m.a.s.l.). (d) Water levels simulated for the 2000–2011 period.

618 Figure 8: Module 4 - Inverse modeling of the water level measured in the main karst conduit at Lez
619 (Lez borehole) on a daily time step. (a) Comparison between the observed and modeled water levels
620 for the calibrated period. (b) Hydrograph separation of the four water-level related components of
621 the transfer model (Fig. 2) – piezometric variations are expressed relative to the reference level (H_0 =
622 59.9 m.a.s.l.). (c) Normalized impulse responses of the four components.

623 Figure 9: (a) Comparison between the observed and modeled water levels for the 1974–2010 period.
624 (b) Effective rainfall calculated for the 1974–2010 period. (c) Natural spring discharge (Qn), pumping
625 discharge (Qp), and pumped karst storage flow (Qs) for the 1974–2010 period. (d) Residual spring
626 discharge (Qr). (e) Detail of the transfer model inputs of the water levels measured in the main karst
627 conduit (water levels modeled by the transfer models 2 and 3 (Fig. 2)

628 Figure 10: Cross correlogram of piezometric data used to describe the hydrodynamics of the Lez karst
629 system.

630 Figure 11: Evolution of the average monthly drawdown in terms of the pumped karst storage
631 volume.

632 Figure 12: Evolution of the various annual volumes of water for the 1974–2010 period. The evolution
633 of the Vs/Vp ratio is plotted at annual scale.

634 Figure 13: (a) Trends of the various volumes of water (average interannual monthly for the 1983–
635 2010 period). The trends of the Vs/Vp and Vs/Vn ratios calculated for the 1983–2010 period are
636 plotted at monthly scale (b, c). The box plots of the Vs/Vp and Vs/Vn ratios are given for the summer
637 months (d and e).

638

References

Aquilina L., Ladouche B., Doerfliger N., 2005. Recharge processes in karstic systems investigated through the correlation of chemical and isotopic composition of rain and spring waters. Appl.Geochem. 20(12):2189-206.

Aquilina L., Ladouche B., Doerfliger N., 2006. Water storage and transfer in the epikarst of karstic systems during high flow periods. Journal of Hydrology 327(3-4):472-85.

Avias J., 1992. Contrôles Géologiques des systèmes aquifères karstiques (s.a.k) de type méditerranéen : l'exemple du S.A.K de la source du Lez-France-(Karstic aquifers of Mediterranean type, geological controls : Lez Spring (North-Montpellierant karsts, France) example. Hydrogeology of Selected Karst Regions, AIH, Volume 13:89-113.

Avias J., 1995 - Gestion active de l'exsurgence karstique de la source du Lez (Hérault, France) 1957-1994. Hydrogéologie 1:113-127.

Bakalowicz M., 2005. Karst groundwater; a challenge for new resources. Hydrogeol. J. 13(1):148-60.

Bérard P., 1983. Alimentation en eau de la Ville de Montpellier. Captage de la source du Lez, commune de St-Clément (Hérault). Etude des relations entre la source et son réservoir aquifère. Rapport n°2, Définition des unités hydrogéologiques. BRGM Report 83 SGN 325 LRO, 27 p.

Birk S, Liedl R, Sauter M (2000) Characterization of gypsum aquifers using a coupled continuum-pipe flow model. In: Stauffer F, Kinzelbach W, Kovar K, Hoehn E (eds) Calibration and reliability in groundwater modelling, vol 265. IAHS Publication, Idyllwild, pp 16–21

Birk S., Liedl R., Sauter M., Teutsch G., 2003. Hydraulic boundary conditions as a controlling factor in karst genesis: A numerical modeling study on artesian conduit development in gypsum. Water Resources Research 39, Art. No. 1004.

661 Clauzon G., Suc J.P., Popescu S.M., Marunteanu M., Rubino J.L., Marinescu F., Melinte M.C., 2005. Influence of
662 Mediterranean sea-level changes on the Dacic Basin (Eastern Paratethys) during the late Neogene: the
663 Mediterranean Lago facies deciphered. Basin Research 17:487-462.

664 Conroux Y., 2007. Caractérisation du fonctionnement hydrodynamique de l'aquifère karstique du Lez à l'état
665 naturel. Mémoire Master 2, Univ. Avignon 2, 151 p.

666 Cornaton F. and Perrochet P., 2002. Analyticial 1D dual-porosity equivalent solution to 3D discrete single-
667 continuum models. Application to karstic spring hydrograph modelling. Journal of Hydrology, 262, 165-176

668 Denic-Jukic V., Jukic D., 2003. Composite transfer functions for karst aquifers. Journal of Hydrology 274:80-94.

669 Dietrich C.R., Chapman T.G., 1993. Unit graph estimation and stabilization using quadratic programming and
670 difference norms. Water Resour Res. 29(8):2629-2635.

671 Dorfliger N., Fleury P., Ladouche B., 2009. Inverse Modeling Approach to Allogenic Karst System
672 Characterization. Ground Water 47(3):414-26.

673 Doherty J. and Skahill B.E., 2006. An advanced regularization methodology for use in watershed model
674 calibration. Journal of Hydrology 327, 564– 577, doi:10.1016/j.jhydrol.2005.11.058

675 Dreiss S.J., 1983. Linear unit-response functions as indicators of recharge areas for large karst springs. J. Hydrol.
676 61:31–44.

677 Drogue C., Grillot J.C., 1976. Structure geologique et premieres observations piezometriques a la limite du sous-
678 systeme karstique de Terrieu (Perimetre experimental). Ann. Sc. Univ. Besancon 25:195-210.

679 Fleury P., Ladouche B., Conroux Y., Jourde H., Dörfliger N., 2008. Modelling the hydrologic functions of a karst
680 aquifer under active water management – the Lez spring. Journal of Hydrology 365:235–243.
681 doi :10.1016/j.jhydrol.2008.11.037

682 Goldscheider N. and Drew D, 2007. Methods in Karst Hydrogeology. Taylor & Francis. International
683 Contributrions to Hydrogeology

684 Guilbot A., 1975. Modélisation des écoulements d'un aquifer karstique (liaison plui debit). Applications aux
685 bassins de Saugras et du Lez. Thesis, Université Montpellier II Sciences et Techniques du Languedoc, 110 p.

686 Jukić D., Denić-Jukić V., 2009. Groundwater balance estimation in karst by using a conceptual rainfall–runoff
687 model. Journal of Hydrology 373(3-4):302-315.

688 Karam Y., 1989. Essai de modélisation des écoulements dans un aquifère karstique. Exemple de la source du
689 Lez (Hérault, France). Thesis, Université Montpellier II Sciences et Techniques du Languedoc, 210 p.

690 Lacas J.L., 1976. Introduction à la méthodologie d'étude et d'utilisation des champs hydrothermiques des
691 aquifères karstiques: d'après l'exemple du site de l'exsurgence de la source du Lez (Hérault, France). Université
692 Montpellier II Sciences et Techniques du Languedoc, CERGA. 68 p.

693 Liedl R., Sauter M., Hückinghaus D., Clemens T., Teutsch G., 2003. Simulation of the development of karst
694 aquifers using a coupled continuum pipe flow model. Water Resources Research 39, Art. No. 1057.

695 Long A. J. and Mahler B. J. (2013).Prediction, time variance, and classification of hydraulic response to recharge
696 in two karst aquifers. Hydrol. Earth Syst. Sci., 17, 281–294,doi:10.5194/hess-17-281-2013

697 Mangin A., 1975 - Contribution à l'étude hydrodynamique des aquifères karstiques (Contribution to
698 hydrodynamic study of karstic aquifers) Thèse de Docteur en Sciences, Université de Dijon ;Annales de
699 Speléologie, 1974,29,3, pp283-332 ;1974,29,4, pp495-601 ;1975 , 30, 1, pp21-124.

700 Marechal J.C., Ladouche B., Doerfliger N., Lachassagne P., 2008. Interpretation of pumping tests in a mixed flow
701 karst system, Water Resources Research 44(5): doi: 10.1029/2007WR006288

702 Martínez-Santos P., Andreu J.M., 2010. Lumped and distributed approaches to model natural recharge in
703 semiarid karst aquifers. Journal of Hydrology 388(3–4):389-98. doi:10.1016/j.jhydrol.2010.05.018
704 Mazzili N. (2011). Sensibilité et incertitude de modélisation sur les bassins versants a forte composante
705 karstique, phD thesis, Université Montpellier II, Sciences et Techniques du Languedoc, 210p

706 Mazzilli N., Guinot V., & Jourde H. Sensitivity analysis of conceptual model calibration to initialisation bias
707 (2011). Application to karst spring discharge models. Advances in Water Resources 42(8), 1-16.
708 doi:10.1016/j.advwatres.2012.03.020.

709 Moussu F., Oudin L., Plagnes V, Mangin A.and Bendjoudi H., 2011. A multi-objective calibration framework for
710 rainfall–discharge models applied to karst systems Journal of Hydrology 400 364–376.
711 doi:10.1016/j.jhydrol.2011.01.047

712 Nash J.E., Sutcliffe J.V., 1970. River flow forecasting through conceptual models part I -A discussion of
713 principles. Journal of Hydrology 10(3):282-290.

714 Padilla A. and Antonio Pulido-Bosch A., 2008.Simple procedure to simulate karstic aquifers. Hydrol. Process. 22,
715 1876–1884. doi: 10.1002/hyp.6772

716 Paloc H., 1979. Alimentation en eau de la ville de Montpellier. Captage de la source du Lez, commune de St.
717 Clément (Hérault). Etude documentaire préalable à l'établissement des périmètres de protection. BRGM Note
718 de synthèse 79SGN319LRO, 47p.

719 Paloc H., 1987. Première évaluation des capacités de production d'eau par pompage du siphon amont de la
720 grotte dite "Du Grand Boulidou". Commune des Matelles (Hérault). BRGM Report 87SGN604LRO, 44p.

721 Pinault J.L., 2001. Manuel utilisateur de TEMPO, logiciel de traitement et de modélisation des séries
722 temporelles en hydrogéologie et en hydrogéochimie. BRGM Report RP-51459-FR, 221 p.

723 Pinault J.L., Pauwels H., Cann C., 2001a. Inverse modeling of the hydrological and the hydrochemical behavior
724 of hydrosystems; application to nitrate transport and denitrification. Water Resour.Res. 37(8):2179-90.

725 Pinault J.L., Plagnes V., Aquilina L., Bakalowicz M., 2001b. Inverse modeling of the hydrological and the
726 hydrochemical behavior of hydrosystems; characterization of karst system functioning. Water Resour. Res.
727 37(8):2191-204.

728 Pinault J.L, Doerfliger N., Ladouche B., Bakalowicz M., 2004. Characterizing a coastal karst aquifer using an
729 inverse modeling approach; the saline springs of Thau, southern France. Water Resour. Res. 40(8):17.

730 Pinault J.L, Amraoui N., Golaz C., 2005. Groundwater-induced flooding in macropore-dominated hydrological
731 system in the context of climate changes. Water Resour. Res. 41(5): W05001, doi:10.1029/2004WR003169.

732 Pinault J.L, Schomburgk S, 2006. Inverse modeling for characterizing surface water/groundwater exchanges.
733 Water Resour.Res. 42(8): W08414, doi:10.1029/2005WR004587.

734 Pinault J.L, Allier D, 2007. Regionalization of rainfall for broad-scale modeling; an inverse approach. Water
735 Resour.Res. 43(9): W09422, doi:10.1029/2006WR005642,.

736 Sivapalan M., 2003. Prediction in ungauged basins: a grand challenge for theoretical hydrology. Hydrol. Process.
737 17:3163–3170. doi: 10.1002/hyp.5155

738 Teutsch G., Sauter M., 1998. Distributed parameter modeling approaches in karst-hydrological investigations.
739 Bull. Hydrogéol. 16:99-109.

740 Thiery D., Berard P. & Camus A., 1983. Captage de la source du Lez : étude des relations entre la source et son
741 réservoir aquifère*. Ed. BRGM, 83 SGN 167 LRO, 95 pp.*

742 Tikhonov A., Arsenine V., 1976. Méthodes de résolution de problèmes mal posés. MIR, Moscow.

743 Tikhonov A.N., Goncharsky A.V. (Eds.), 1987. Ill-Posed Problems in the Natural Sciences. MIR, Moscow.

744 Von Asmuth, J. R., Bierkens M. F. P. and Maas K., 2002. Transfer function-noise modeling in continuous time
745 using predefined impulse response functions, Water Resour. Res., 38(12), 1287, doi: 10.1029/2001WR001136

746

747

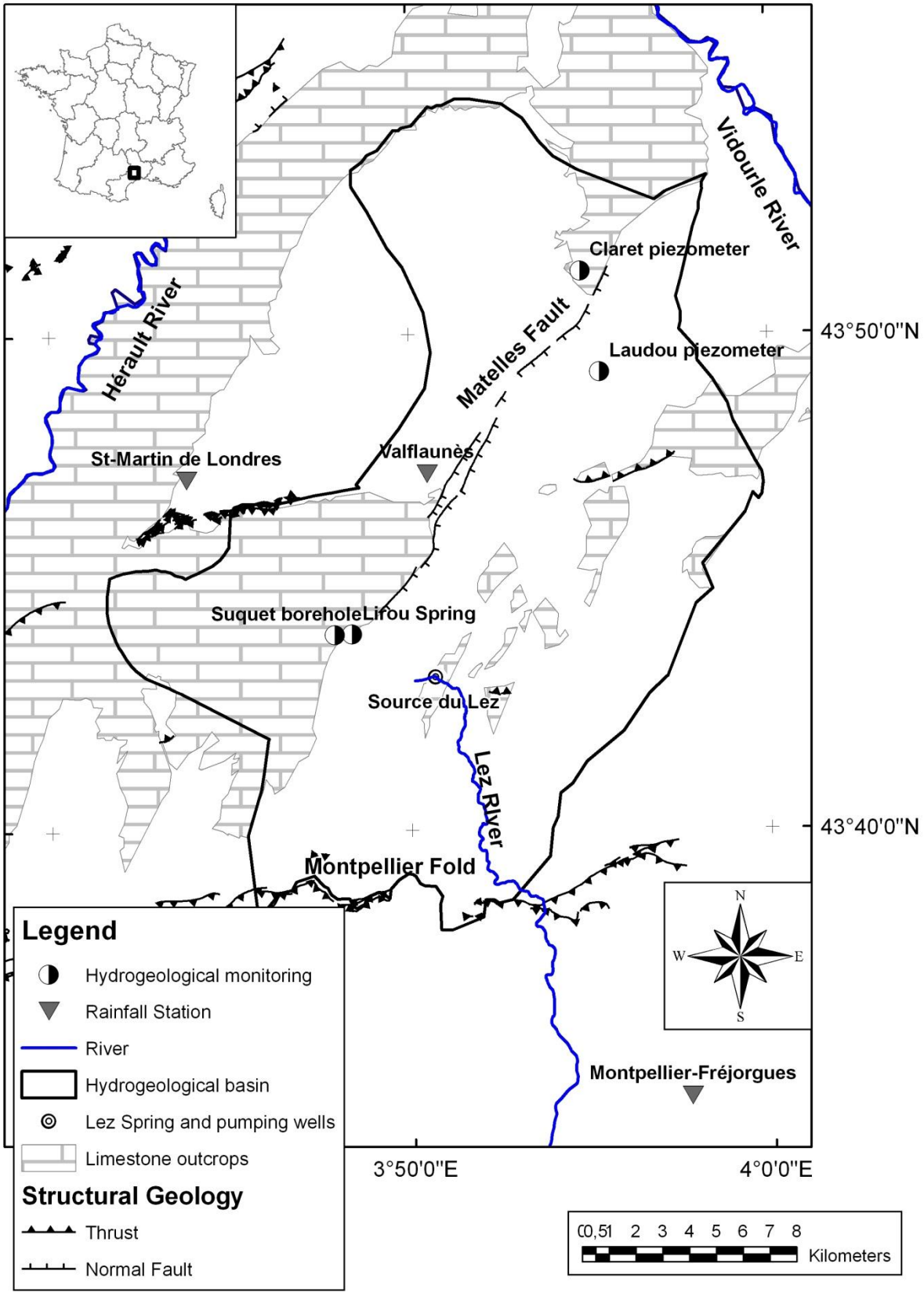

748

749 Figure 1.

750

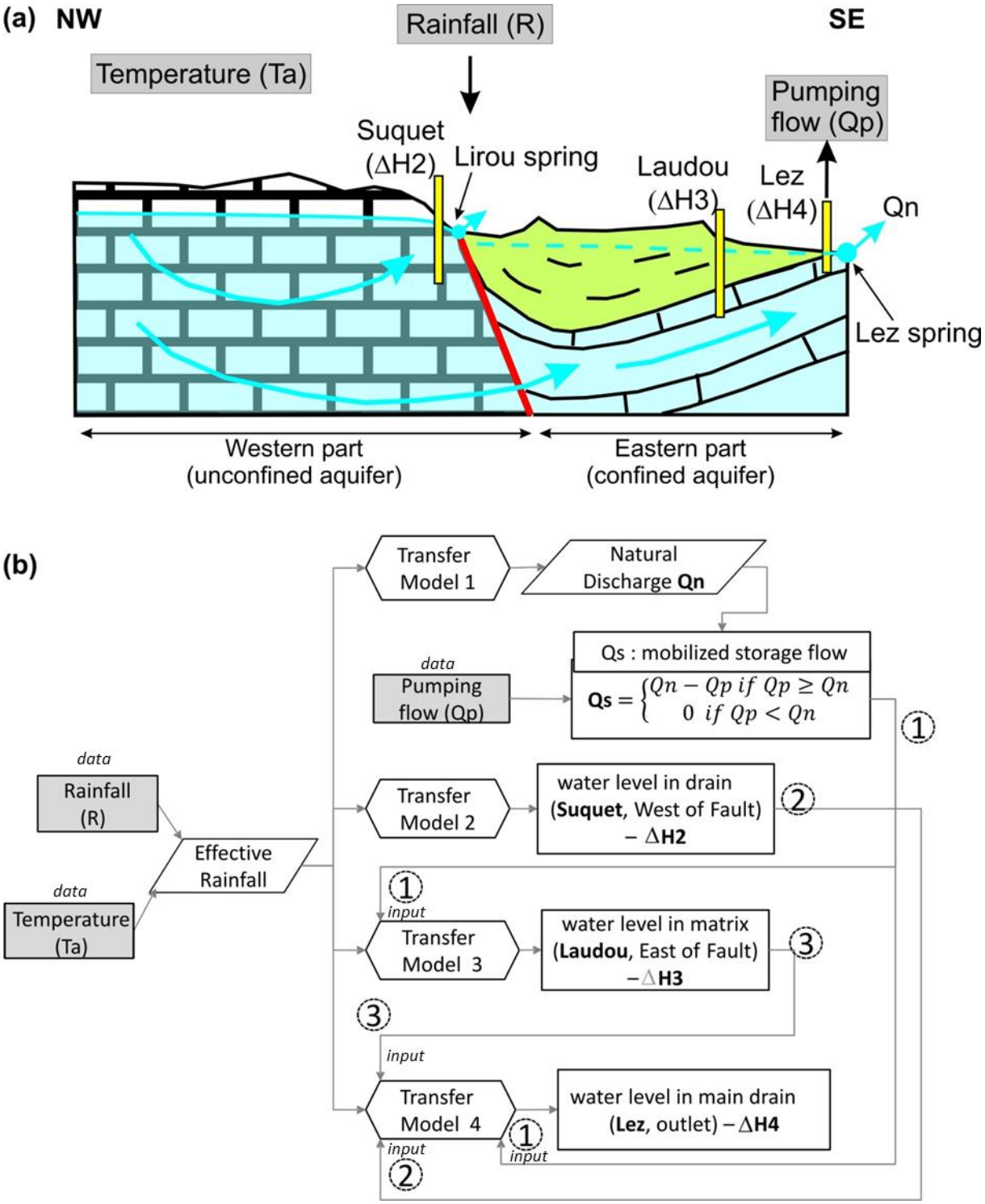

751

752 Figure 2

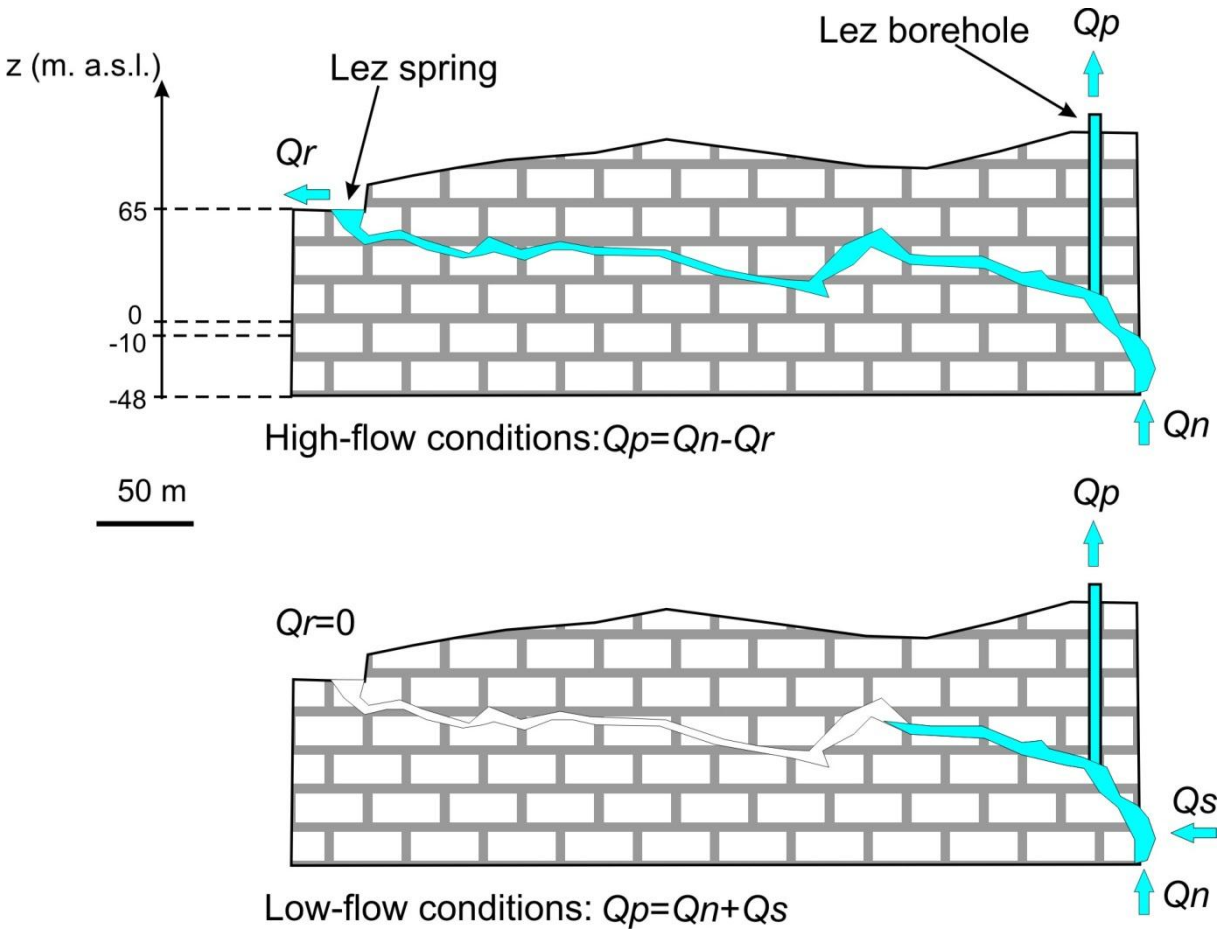

753

754

755 Figure 3

756

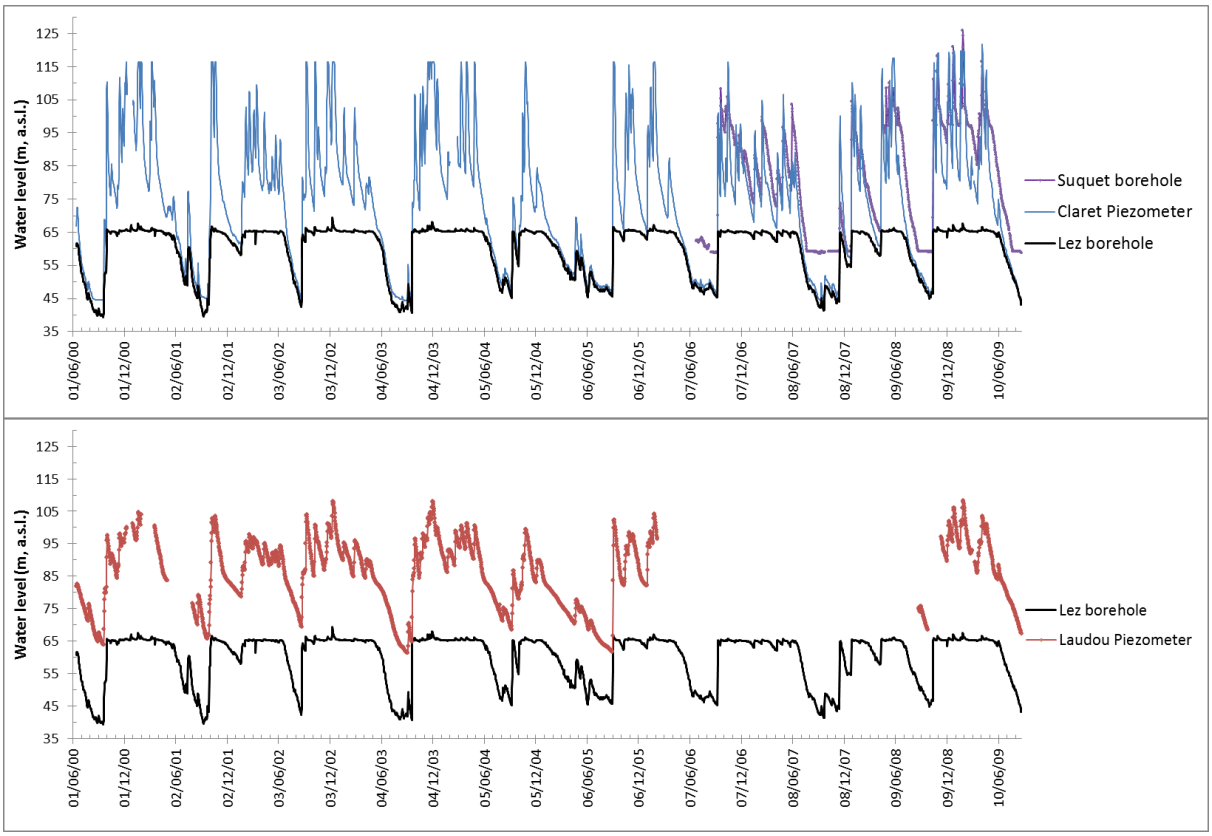
Water level (m, a.s.l.)
125
115
105
95
85
75
65
55
45
35
01/06/00
01/12/00
02/06/01
02/12/01
03/06/02
03/12/02
04/06/03
04/12/03
05/06/04
05/12/04
06/06/05
06/12/05
07/06/06
07/12/06
08/06/07
08/12/07
09/06/08
09/12/08
10/06/09
Suquet borehole
Claret Piezometer
Lez borehole
Water level (m, a.s.l.)
Lez borehole
Laudou Piezometer

Figure 4

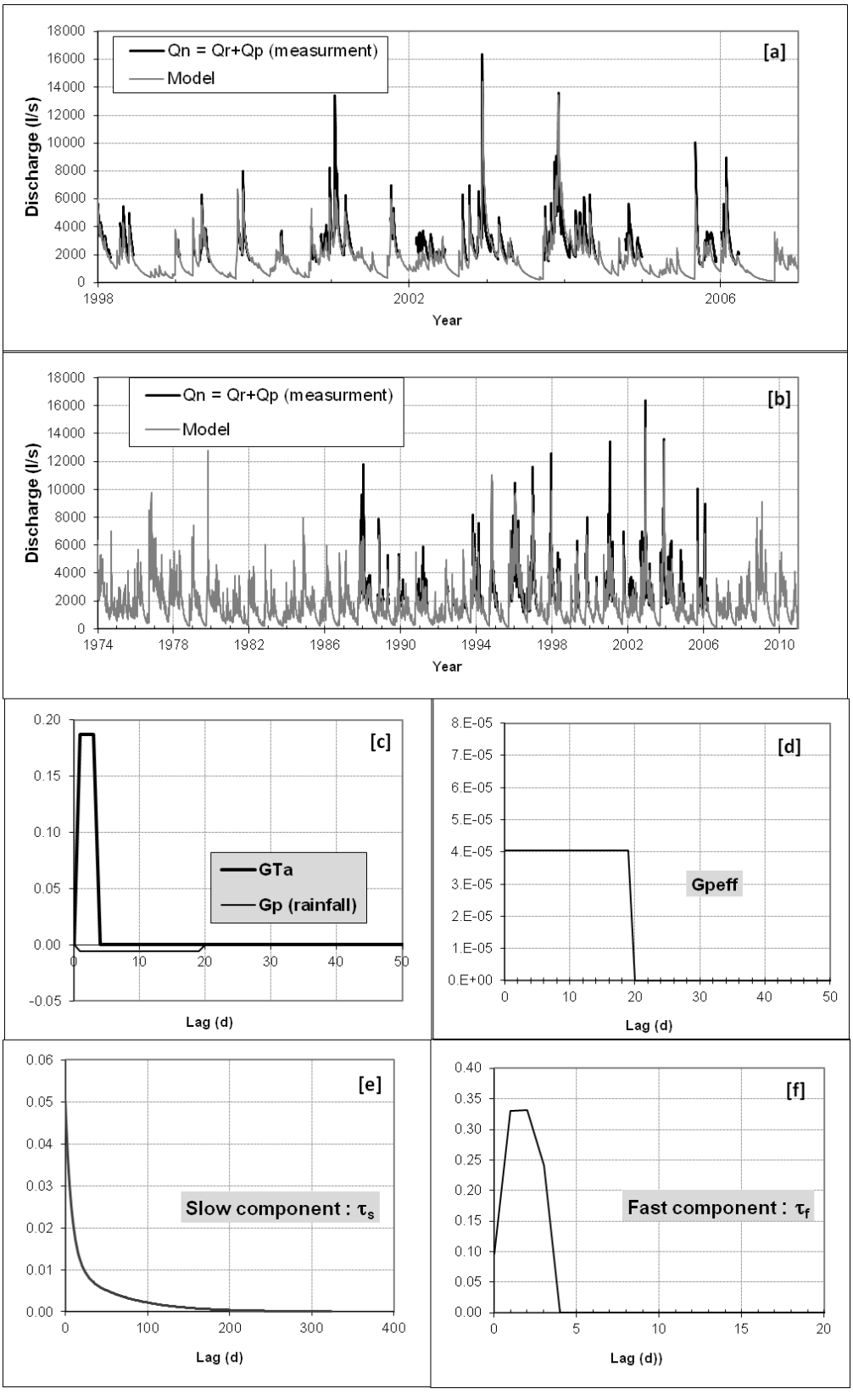

761

762 Figure 5

763

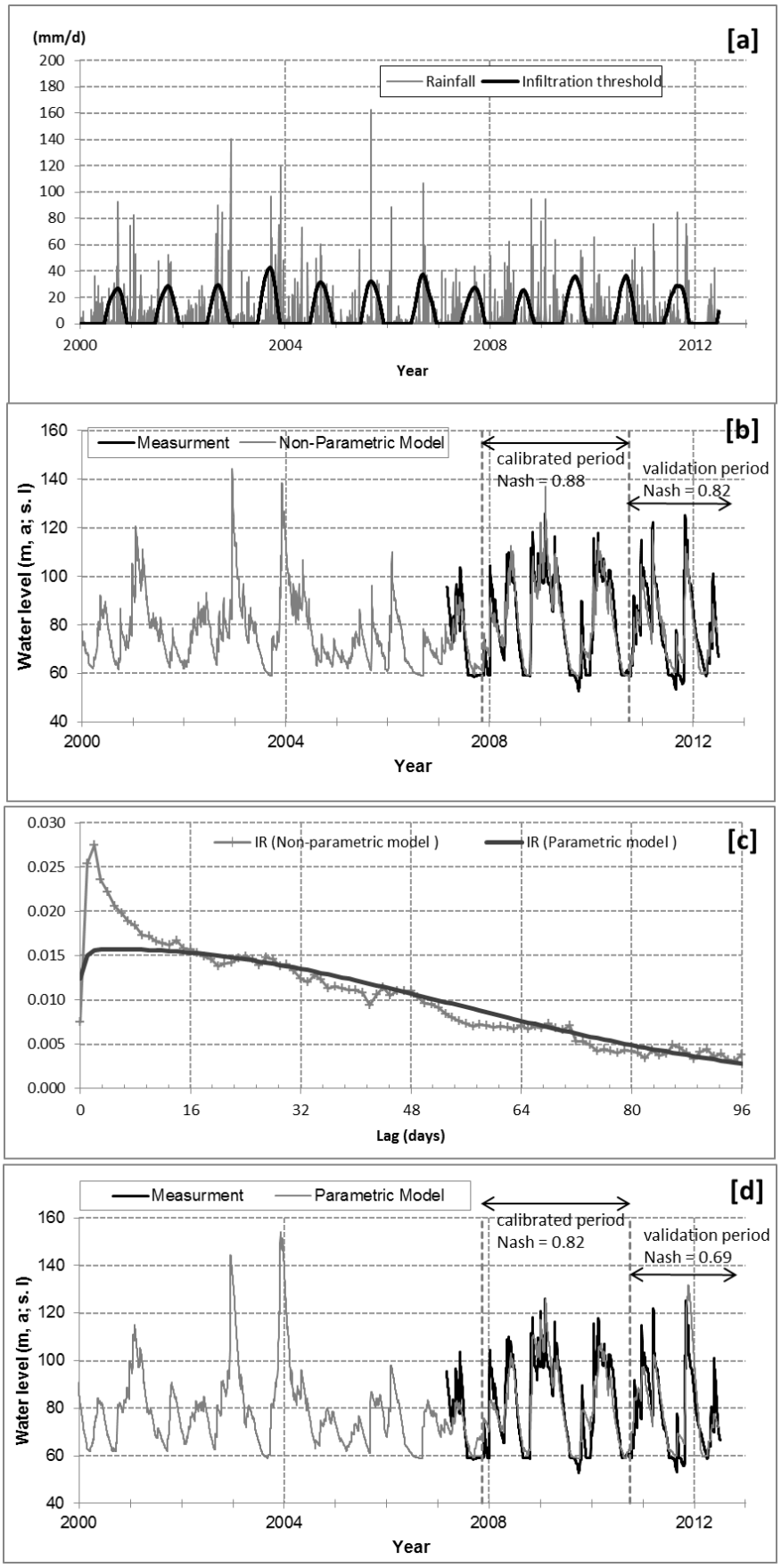

764

765 Figure 6

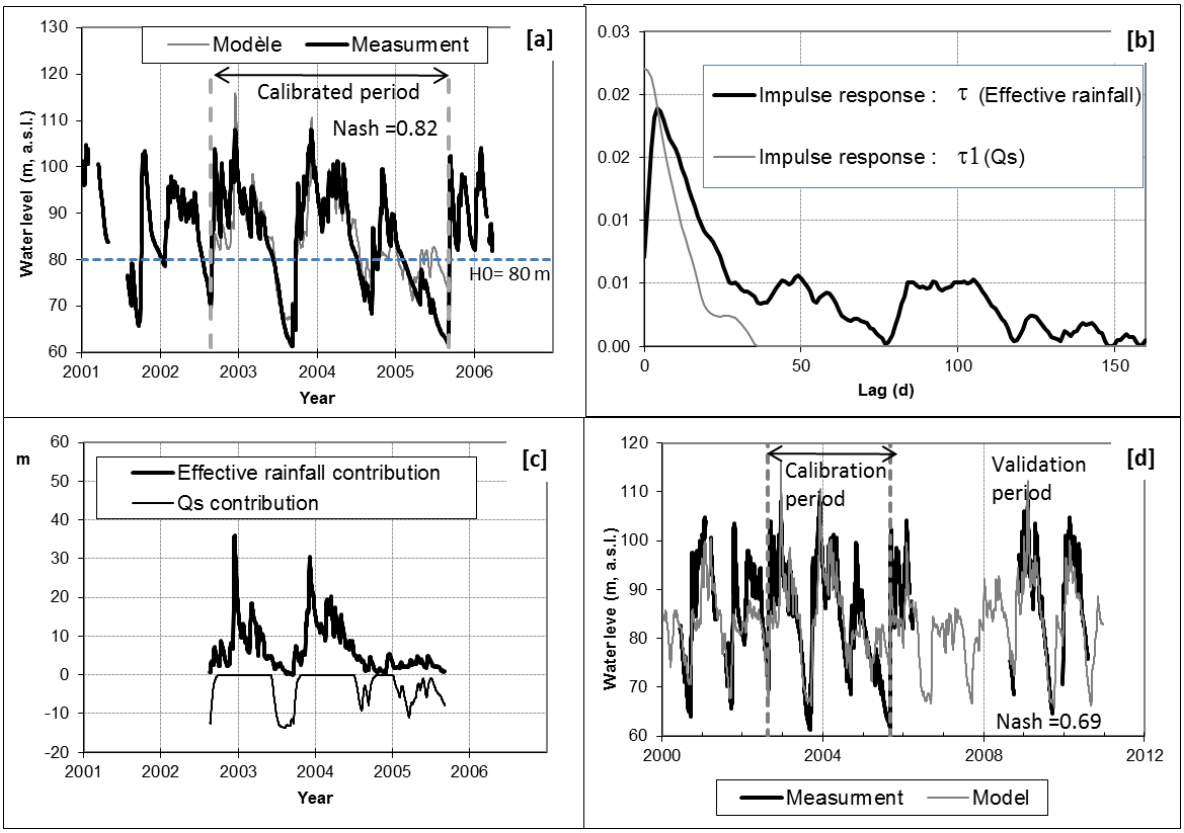

766

767 Figure 7

768

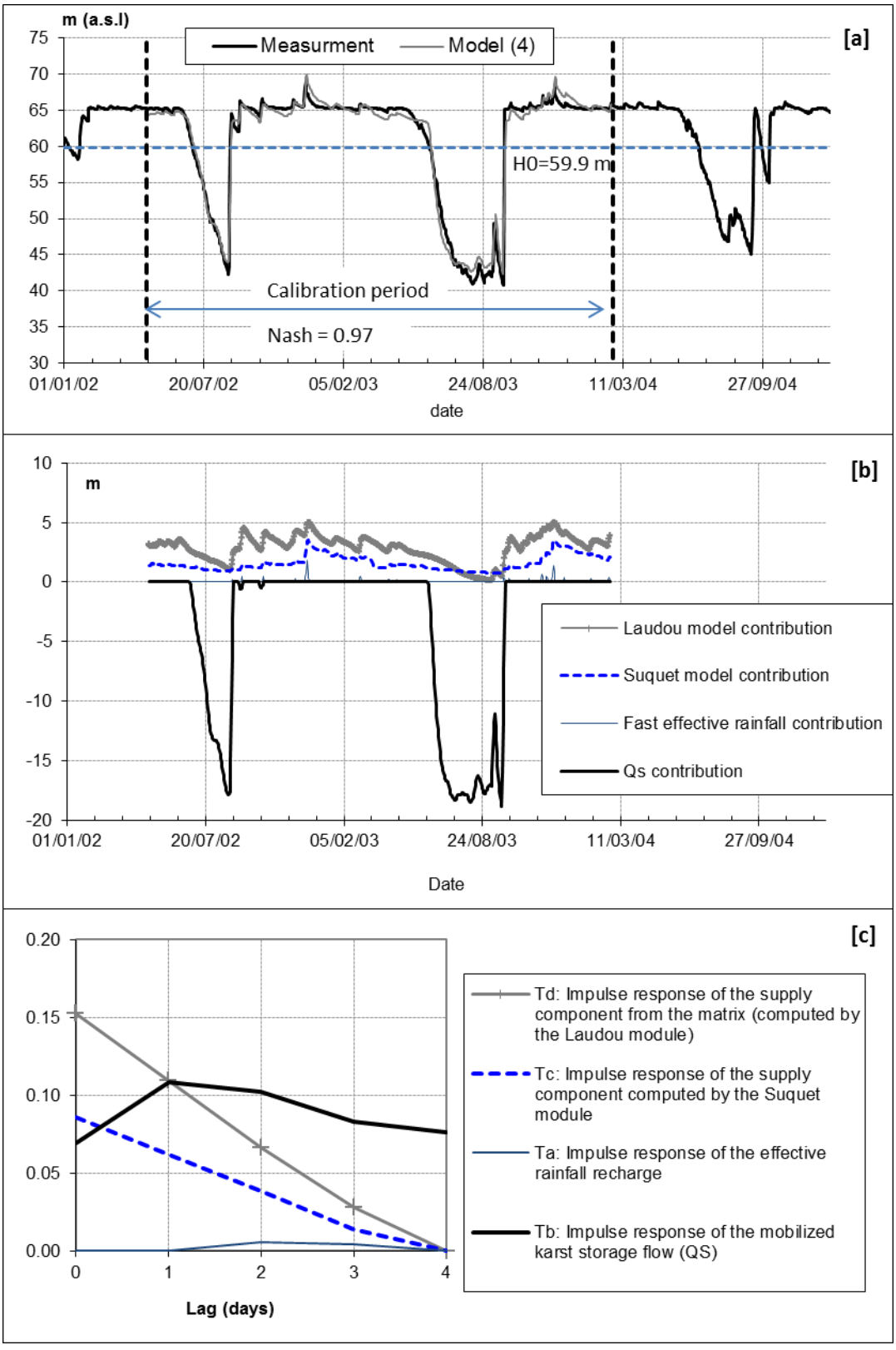
m (a.s.l)
Measurment
Model (4)
[a]
H0=59.9 m
Calibration period
Nash = 0.97
date
[b]
m
Laudou model contribution
Suquet model contribution
Fast effective rainfall contribution
Qs contribution
Date
[c]
Td: Impulse response of the supply component from the matrix (computed by the Laudou module)
Tc: Impulse response of the supply component computed by the Suquet module
Ta: Impulse response of the effective rainfall recharge
Tb: Impulse response of the mobilized karst storage flow (QS)
Lag (days)

Figure 8

772

773

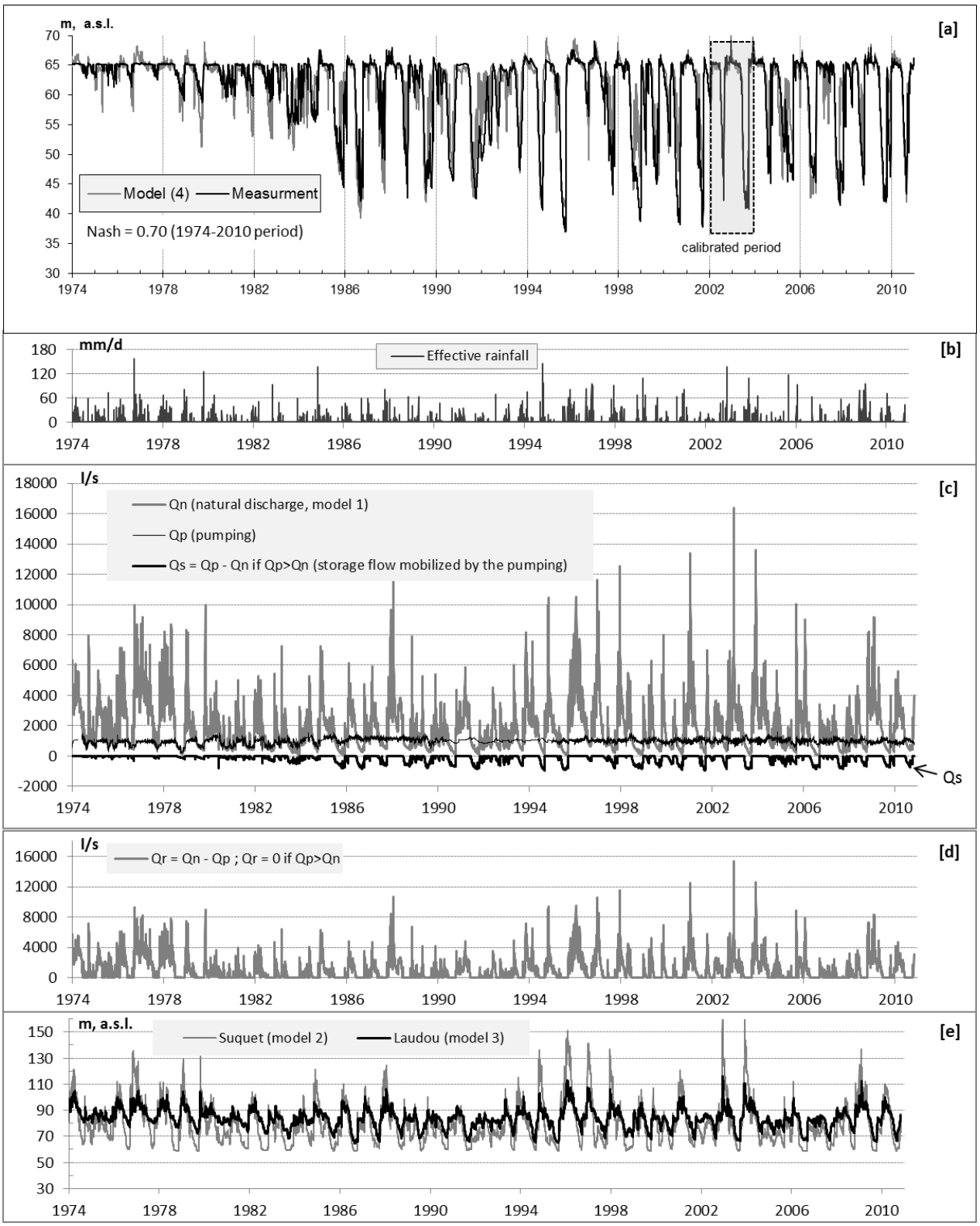

774

775 Figure 9.

776

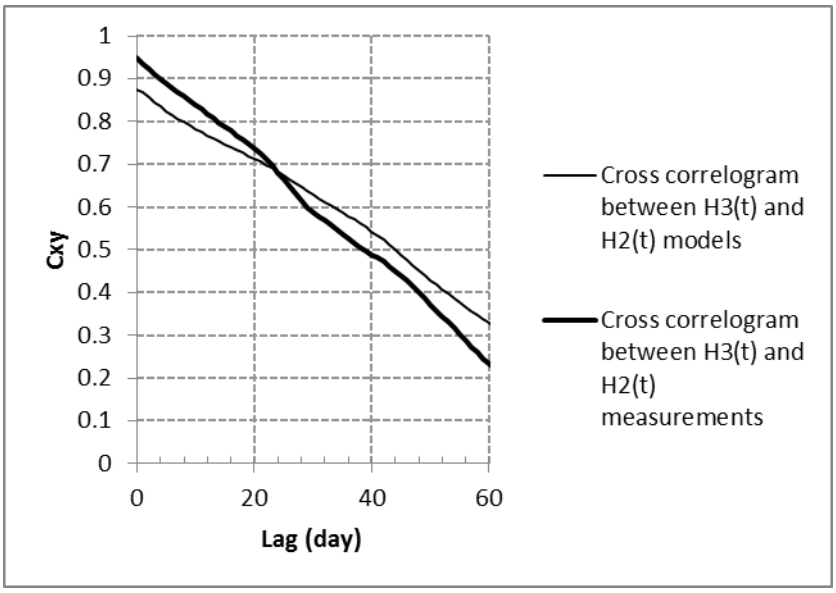

777

778 Figure 10

779

780

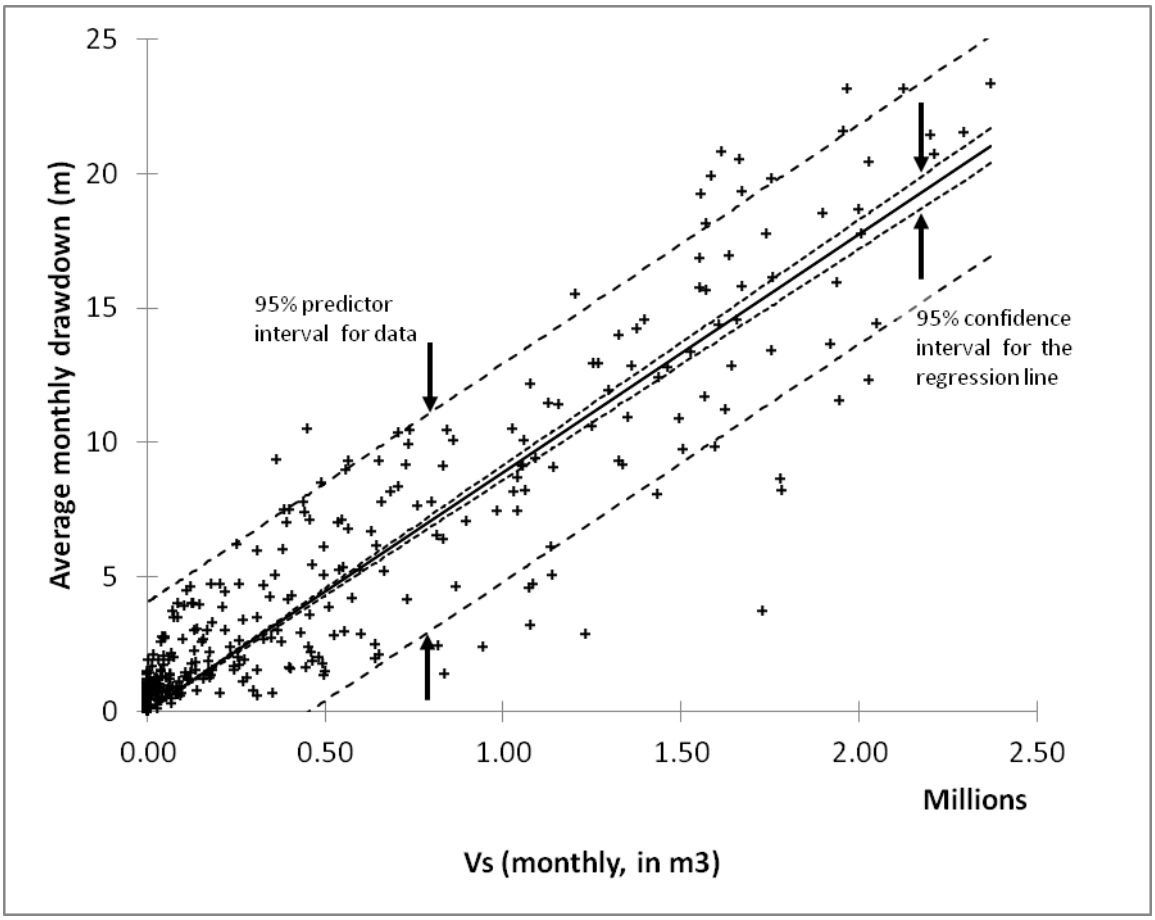

781

782 Figure 11

783

784

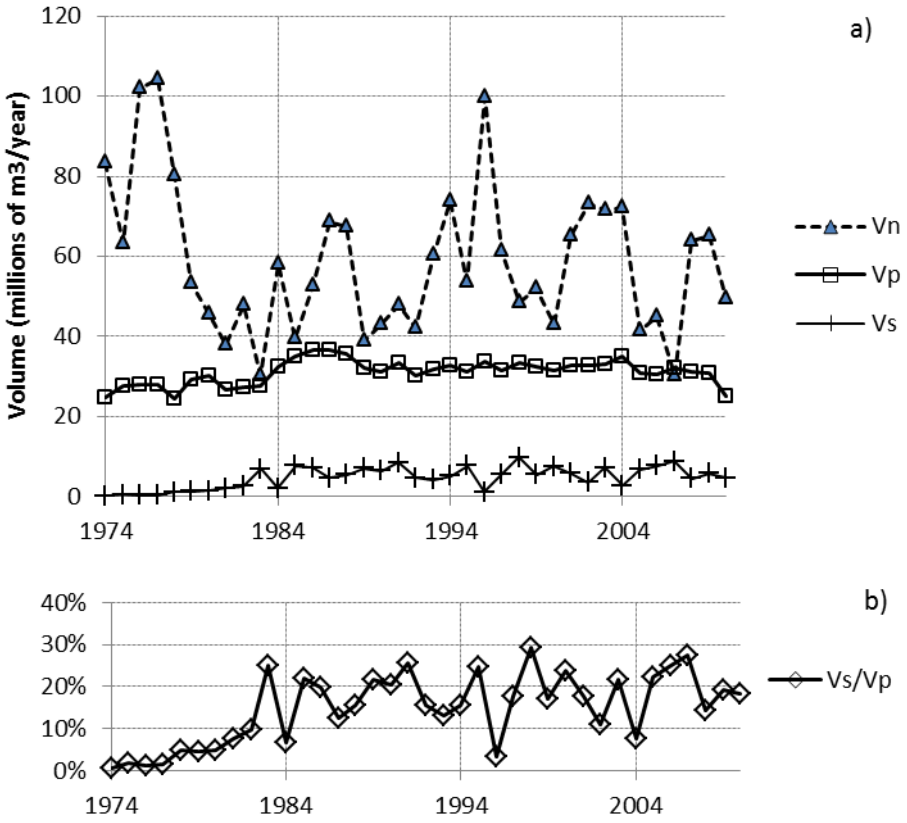

785

786 Figure 12

787

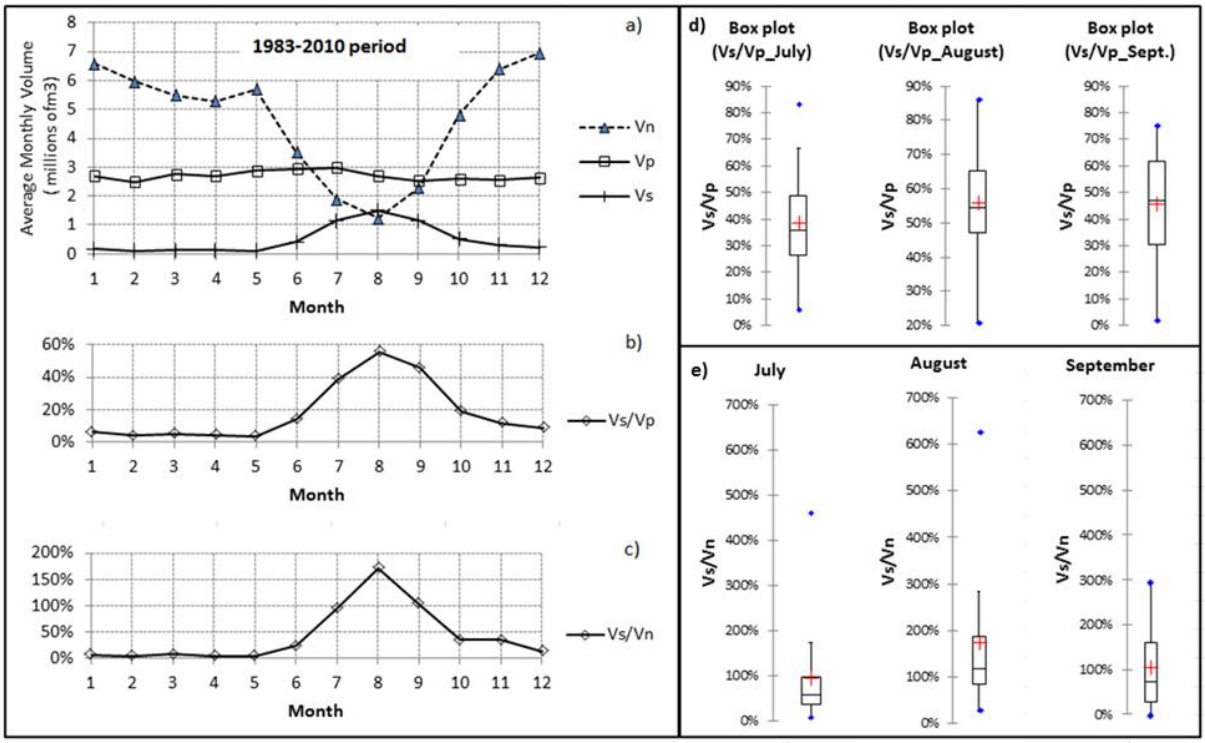
a)
1983-2010 period
Average Monthly Volume (millions of m3)
Month
Vn
Vp
Vs
b)
Vs/Vp
c)
Vs/Vn
d)
Box plot (Vs/Vp_July)
Box plot (Vs/Vp_August)
Box plot (Vs/Vp_Sept.)
e)
July
August
September

Figure 13.